2. Properties of Solid-State Laser Materials

Materials for laser operation must possess sharp fluorescent lines, strong absorption bands, and a reasonably high quantum efficiency for the fluorescent transition of interest. These characteristics are generally shown by solids (crystals or glass) that incorporate in small amounts elements in which optical transitions can occur between states of inner, incomplete electron shells. Thus the transition metals, the rare earth (lanthanide) series, and the actinide series are of interest in this regard. The sharp fluorescence lines in the spectra of crystals doped with these elements result from the fact that the electrons involved in transitions in the optical regime are shielded by the outer shells from the surrounding crystal lattice. The corresponding transitions are similar to those of the free ions.

Most solid-state lasers emit radiation in the spectral region ranging from 400 nm to 3 μm that is based on 4f–4f transitions of rare earth and 3d–3d transitions of transition-metal-doped crystals. The spectroscopic properties of the laser transition determine the way the laser system may be designed and operated. The laser transition is characterized by its upper level lifetime τ_f, emission cross section σ, and gain bandwidth $\Delta\nu$.

For the continuous wave (cw) operation, the threshold for laser action is inversely proportional to the product $(\sigma\tau_f)$. Therefore, the value of $\sigma\tau_f$ is an important criterion whether a laser can be operated in the cw mode. For pulsed operation, the threshold becomes independent of the lifetime when the pump pulse duration is much shorter than τ_f. In Q-switching, energy storage time prior to Q-switching is limited by the upper level lifetime, while the emission cross section determines the magnitude of the gain. A long upper state lifetime permits the use of a long pump pulse, thereby increasing energy storage. This is particularly important for diode-pumped lasers where the pump source is power-limited, rather than energy-limited.

The gain bandwidth $\Delta\nu$ limits the tuning range of the laser system and determines the minimum pulsewidth that can be achieved in a mode-locked laser. Transition-metal ions mostly exhibit broadband emission, which offers broad tunability and generation of extremely short pulses.

In addition to a favorable combination of parameters describing the laser transition, a viable laser material must also possess pump bands that are within the emission spectrum of readily available pump sources, such as arc lamps and diode laser arrays. A broad absorption band is required of efficient arc lamp pumping, whereas a relatively narrow spectral pump band is acceptable for diode pumping.

The location of the lower laser level within the energy level diagram also has a profound impact on the pump source requirement. As explained in the previous

chapter, we have to distinguish between three- and four-level laser systems. In a four-level system, the lower laser level is above the ground state by an energy gap $\Delta E \gg kT$. Under these conditions the lower laser level is not thermally populated and it requires less energy to generate population inversion compared to a three-level laser where laser action terminates at the ground level and ground-state absorption overlaps laser emission.

In between the three- and four-level systems are the so-called quasi-three-level or quasi-four-level lasers. In these lasers the laser transition terminates at a level close to the ground level and is, therefore, thermally populated. The disadvantage of three-level and quasi-three-level lasers of requiring high pump intensities to reach threshold can be overcome to some extent if the laser material has other favorable characteristics which will be discussed later in this chapter.

The three principal elements leading to gain in a solid-state laser are as follows:

- *The host material* with its macroscopic mechanical, thermal, and optical properties, and its unique microscopic lattice properties.
- *The activator/sensitizer ions* with their distinctive charge states and free-ion electronic configurations.
- *The optical pump source* with its particular geometry, spectral irradiance, and temporal characteristic.

These elements are interactive and must be selected self-consistently to achieve a given system performance.

In this chapter we consider the properties of various host materials and activator/sensitizer combinations and we will describe some of the features of the most prominent laser materials.

The ruby laser, still in use today, provides a good illustration of a three-level system.

Nd:YAG, because of its high gain and good thermal and mechanical properties, is by far the most important solid-state laser for scientific, medical, industrial, and military applications. Nd:glass is important for laser fusion drivers because it can be produced in large sizes. Nd:YLF is a good material for a number of applications; the crystal exhibits lower thermal birefringence and has a higher energy storage capability (due to its lower gain coefficient) compared to Nd:YAG. The crystal Nd:YVO_4 has become a very attractive material for small diode-pumped lasers because of its large emission cross section and strong absorption at 809 nm.

The Nd:Cr:GSGG laser is an example of the application of a codoped laser material where the Cr^{3+} ions provide broad absorption bands for efficient flashlamp pumping and the energy absorbed by Cr^{3+} is transferred to the upper laser level of the Nd^{3+} ions.

Highly doped Er:YAG emits at a wavelength around 3 μm. This is an attractive wavelength for certain medical applications. Er:glass is of special importance because the laser output at 1.55 μm is in the eye-safe region of the spectrum.

The group of tunable lasers includes alexandrite, Ti:sapphire, and Cr:LiSAF. Laser emission is achieved by the 3d-electron of Cr^{3+} or Ti^{3+}. In these "vibronic" lasers the emission of photons is closely coupled to the emissions of phonons in the

crystal lattice (vibrational quanta). Broad wavelength tunability is achieved because the energy of the laser transition can be partitioned between photons and phonons in a continuous fashion. In the Tm:YAG laser the considerable phonon broadening and high multiplicity of the Stark level of the 4f-electron provides tunability around 2 μm.

The Yb:YAG laser is an example of a quasi-three-level laser. This diode-pumped laser has become a very important system for high power applications in the kilowatt range.

Overviews of laser host materials and active ions, as well as compilations of useful laser and materials parameters, can be found in a number of handbooks and summary articles [2.1–7].

2.1 Overview

The conditions for laser action at optical frequencies were first described by Schawlow and Townes [2.8] in 1958. The first demonstration of laser action by Maiman [2.9] was achieved in 1960 using ruby (Cr^{3+}:Al_2O_3), a crystalline solid system. The next step in the development of solid-state lasers was the operation of trivalent uranium in CaF_2 and divalent samarium in CaF_2.

Laser action in neodymium-doped glass and the first continuously operating crystal laser using Nd^{3+}:$CaWO_4$ were reported in 1961. Since then laser action has been achieved from trivalent rare earths (Nd^{3+}, Er^{3+}, Ho^{3+}, Ce^{3+}, Tm^{3+}, Pr^{3+}, Gd^{3+}, Eu^{3+}, Yb^{3+}), divalent rare earths (Sm^{2+}, Dy^{2+}, Tm^{2+}), transition metals (Cr^{3+}, Ni^{2+}, Co^{2+}, Ti^{3+}, V^{2+}), and the actinide ion U^{3+} embedded in various host materials. Optically pumped laser action has been demonstrated in hundreds of ion-host crystal combinations covering a spectral range from the visible to the mid-infrared.

The exceptionally favorable characteristics of the trivalent neodymium ion for laser action were recognized at a relatively early stage in the search for solid-state laser materials. Thus, Nd^{3+} was known to exhibit a satisfactorily long fluorescence lifetime and narrow fluorescence linewidths in crystals with ordered structures, and to possess a terminal state for the laser transition sufficiently high above the ground state so that cw operation at room temperature was readily feasible. Therefore, this ion was incorporated as a dopant in a variety of host materials, that is, glass, $CaWO_4$, $CaMoO_4$, CaF_2, LaF_3, and so forth, in an effort to make use of its great potential. However, most of these early hosts displayed undesirable shortcomings, either from the standpoint of their intrinsic physical properties or because of the way in which they interacted with the Nd^{3+} ions. Finally, yttrium aluminum garnet (YAG) was explored by Geusic et al. [2.10] as a host for Nd^{3+}, and its superiority to other host materials was quickly demonstrated.

2.1.1 Host Materials

Solid-state host materials may be broadly grouped into crystalline solids and glasses. The host must have good optical, mechanical, and thermal properties to withstand the

severe operating conditions of practical lasers. Desirable properties include hardness, chemical inertness, absence of internal strain and refractive index variations, resistance to radiation-induced color centers, and ease of fabrication.

Several interactions between the host crystal and the additive ion restrict the number of useful material combinations. These include size disparity, valence, and spectroscopic properties. Ideally, the size and valence of the additive ion should match that of the host ion it replaces.

In selecting a crystal suitable for a laser ion host one must consider the following key criteria:

(a) The crystal must possess favorable optical properties. Variations in the index of refraction lead to inhomogeneous propagation of light through the crystal, which results in poor beam quality.
(b) The crystal must possess mechanical and thermal properties that will permit high-average-power operation. The most important parameters are thermal conductivity, hardness, and fracture strength.
(c) The crystal must have lattice sites that can accept the dopant ions and that have local crystal fields of symmetry and strength needed to induce the desired spectroscopic properties. In general, ions placed in a crystal host should have long radiative lifetimes with emission cross sections near 10^{-20} cm^2.
(d) It must be possible to scale the growth of the impurity-doped crystal, while maintaining high optical quality and high yield.

Glasses

Glasses form an important class of host materials for some of the rare earths, particularly Nd^{3+}. The outstanding practical advantage compared to crystalline materials is the tremendous size capability for high-energy applications. Rods up to 1 m in length and over 10 cm in diameter and disks up to 90 cm in diameter and several centimeters thick have been produced. The optical quality is excellent, and glass, of course, is easily fabricated and takes a good optical finish. Laser ions placed in glass generally show a larger fluorescent linewidth than in crystals as a result of the lack of a unique and well-defined crystalline field surrounding the individual active atoms. Therefore, the laser thresholds for glass lasers have been found to run higher than their crystalline counterparts. Also, glass has a much lower thermal conductivity than most crystalline hosts. The latter factor leads to a large thermally induced birefringence and optical distortion in glass laser rods when they are operated at high average powers.

For bulk solid-state lasers, glass doped with Nd^{3+} or Er^{3+} is important and will be discussed in Sects. 2.3.2 and 2.4.2. In fiber oscillators and amplifiers, Er^{3+}-doped and Yb^{3+}-doped glass provides the active medium.

Oxides

A large number of crystalline host materials have been investigated since the discovery of the ruby laser. Crystalline laser hosts generally offer as advantages over glasses their

higher thermal conductivity, narrower fluorescence linewidths, and, in most cases, greater hardness. However, the optical quality and doping homogeneity of crystalline hosts are often poorer, and the absorption lines are generally narrower.

Sapphire. The first laser material to be discovered (ruby laser) employed sapphire as a host. The Al_2O_3 (sapphire) host is hard, with high thermal conductivity, and transition metals can readily be incorporated substitutionally for the Al. The Al site is too small for rare earths, and it is not possible to incorporate appreciable concentrations of these impurities into sapphire. Besides ruby, which is still used today, Ti-doped sapphire has gained significance as a tunable laser material. The properties of ruby and Ti-sapphire will be discussed in Sects. 2.2 and 2.5.2.

Garnets. Some of the most useful laser hosts are the synthetic garnets: yttrium aluminum garnet, $Y_3Al_5O_{12}$ (YAG); gadolinium gallium garnet , $Gd_3Ga_5O_{12}$ (GGG); and gadolinium scandium aluminum garnet, $Gd_3Sc_2Al_3O_{12}$ (GSGG). These garnets have many properties that are desirable in a laser host material. They are stable, hard, optically isotropic, and have good thermal conductivities, which permits laser operation at high average power levels.

In particular, yttrium aluminum garnet doped with neodymium (Nd:YAG) has achieved a position of dominance among solid-state laser materials. YAG is a very hard, isotropic crystal, which can be grown and fabricated in a manner that yields rods of high optical quality. At the present time, it is the best commercially available crystalline laser host for Nd^{3+}, offering low threshold and high gain. The properties of Nd:YAG are discussed in more detail in Sect. 2.3.1.

Besides Nd^{3+}, the host crystal YAG has been doped with Tm^{3+}, Er^{3+}, Ho^{3+}, and Yb^{3+}. Important members of this group of lasers include Yb:YAG, Er:YAG, Tm:YAG, and Nd:Cr:GSGG, which will be discussed in Sects. 2.6, 2.4.1, 2.5.4, and 2.3.3, respectively.

Aluminate. In 1969 a crystal host derived from the same Y_2O_3–Al_2O_3 system as YAG was discovered [2.11]. The crystal yttrium ortho aluminate ($YAlO_3$), termed YAlO or YAP is the 1:1 compound or perovskite phase (YAG is the 3:5 compound or garnet phase). Many physical properties of YAP such as hardness and thermal conductivity are similar to those of YAG. In contrast to YAG, which is cubic and isotropic, YAP is orthorhombic and anisotropic. The anisotropy of the spectral properties of $YAlO_3$ enables one to select crystallographic orientations of the laser rod which optimize particular performance characteristics. Thus rod orientations can be chosen for high gain and low thresholds or, alternatively, for low gain and high energy storage required for Q-switching operation.

The fluorescence in Nd:$YAlO_3$ occurs predominantly in three strong lines at 1.0645, 1.0725, and 1.0795 μm. For light propagating along the *b* axis of the crystal, the gain is maximum at 1.0795 μm and is comparable to that of the 1.064-μm line in Nd:YAG. For a beam propagating along the *c* axis of Nd:$YAlO_3$, the gain is maximum at 1.064 μm, but it is only about one-half of that in Nd:YAG. Laser action in YAP has been achieved with ions including Nd^{3+}, Er^{3+}, Ho^{3+}, and Tm^{3+}.

Despite several major potential advantages of YAP over YAG, such as a polarized output, the capability of accepting a higher concentration of Nd, the possibility of varying gain by changing the rod axis, and lower costs because of faster crystal growth, the material disappeared from the market only 2 years after its introduction. YAP's disadvantages were lower efficiency than expected and erratic performance. It was found, for example, that during the growth process Fe^{3+} impurities enter the single crystal, which increase the absorption loss at 1.06 μm and cause fluorescence quenching. However, over the years it has been possible to improve the optical quality of the YAP crystals and the material is commercially available again. For example, a diode-pumped Nd:YALO laser with 100 W output was reported in [2.12].

Oxysulfide. The application of rare earth oxysulfides as laser host materials has also been explored. The entire oxysulfide series, from lanthanum oxysulfide through lutetium oxysulfide and yttrium oxysulfide, possess the same (uniaxial) crystal structure. Thus, solid solutions of any concentration of rare earth activator in any other rare earth oxysulfide host are possible. Host materials which are transparent from 0.35 to 7 μm include lanthanum, gadolinium, yttrium, and lutetium oxysulfide. Laser action was observed at 1.075 μm for Nd and La_2O_2S. The lasing transition cross section of Nd:LOS was measured to be about one-third of that of Nd:YAG [2.13]. The optical quality of LOS crystals is far below the quality of YAG crystals.

Phosphates and Silicates

Laser oscillations have been produced in crystals of Nd^{3+}-doped calcium fluorophosphate or $Ca_5(PO_4)_3F$. The host crystal has the mineral name fluorapatite, from which the name FAP was coined [2.14]. This material is unique in that the Nd^{3+} fluorescence spectrum is predominantly concentrated in a single narrow and intense line, whereas the absorption spectrum is relatively broad and intense. Fluorapatites have low oscillation thresholds and high slope efficiencies, but they are soft, are susceptible to the formation of color centers, and their low thermal conductivity leads to strong thermal distortions. Because of these latter properties, FAP did not become a popular laser material. In 1972 another apatite became available: silicate oxyapatite or CaLaSOAP. In contrast to FAP, CaLaSOAP is considerably harder; however, its thermal conductivity is nearly equal to that of FAP and is only one-ninth the thermal conductivity of YAG.

The energy storage in Nd:SOAP is about five times that of YAG. In addition to SOAP's high energy storage, the material has the potential that large crystals can be grown inexpensively. Crystals 15 cm long with diameters as large as 1.2 cm have been grown at growth rates of 2–3 mm/h. It was reported that the optical quality of SOAP rods 7.5 by 0.6 cm was comparable to the quality of YAG rods with undetectable scattering and less than 0.5 fringe. The main disadvantages of SOAP are low laser damage threshold and low thermal conductivity. Physical, spectroscopic, and laser characteristics of neodymium-doped silicate oxyapatite are reported in [2.15].

Laser action has been achieved in the neodymium pentaphosphates $YNdP_5O_{14}$, $LaNdP_5O_{14}$, and $ScNdP_5O_{14}$ [2.16–19]. An outstanding property of these materials is

the high gain which can be achieved as a result of the favorable position of the $^4I_{15/2}$ manifold relative to the upper laser states. As a result of the high gain, cw oscillation at room temperature has been obtained in $ScNdP_5O_{14}$ with a pump power of only 4 mW, using an argon laser as a pump source [2.19].

Tungstates, Molybdates, Vanadates, and Beryllates

$CaWO_4$ was the most popular material for Nd before YAG became commercially available. The rare earth substitutes for Ca, but only in the trivalent oxidation state, and hence charge compensation is needed. The material is very prone to fracture, even when well annealed, and thus considerable care is required when the boules are being fabricated into laser rods. The thermal conductivity is three to four times greater than that of the glasses.

Sodium rare earth molybdates and tungstates have served as host materials for active ions. In these materials, which are similar to $CaWO_4$ and $CaMoO_4$, one-half of the calcium atoms are randomly replaced with sodium and the other half with rare earth. Laser action has been observed from Nd^{3+} in $NaLa(MoO_4)_2$ and $NaGd(WO_4)_2$ and from $NaNd(WO_4)_2$. Interest in Nd:$NaLa(MoO_4)_2$ stems from the fact that this material has a low gain, intermediate to Nd:glass and Nd:YAG, and thus is capable of higher efficiencies than the former material and greater energy storage than the latter material. The thermal conductivity of Nd:$NaLa(MoO_4)$ is three times that of the Nd:glass. However, the lower thermal conductivity and the higher thermal expansion coefficient of Nd:$NaLa(MoO_4)_2$ as compared to Nd:YAG result in a Nd:$NaLa(MoO_4)_2$ laser rod having much greater thermal stress than a Nd:YAG rod when both are subjected to the same average input power during lasing action.

Nd^{3+}-doped yttrium orthovanadate (YVO_4) was known for a long time as a material having a low threshold [2.21]. However, early studies of this crystal were hampered by severe crystal growth problems, and as a result YVO_4 was discarded as a host. With the emergence of diode pumping, Nd:YVO_4 has become an important solid-state laser material because it has very attractive features, such as a large stimulated emission cross section and a high absorption of the pump wavelength. Also the growth problem has been overcome for the small crystals required with diode pump sources. Details of this laser crystal will be discussed in Sect. 2.3.5.

Gadolinium vanadate (Nd:$GdVO_4$) is an interesting laser crystal because it has a thermal conductivity similar to that of Nd:YAG and an absorption and emission cross section similar to that of Nd:YVO_4. Recently high quality Nd:$GdVO_4$ crystals have been grown with a floating zone method [2.20].

A candidate of the beryllates is Nd^{3+}-doped lanthanum beryllate (Nd:$La_2Be_2O_5$) [2.22]. Since La^{3+} is the largest of the rare earth ions, $La_2Be_2O_5$ (BEL) has large distribution coefficients for other trivalent rare earth ions. For this reason boules of BEL with high concentrations of rare earth ions are much more readily grown than are YAG and other hosts based on the yttrium ion. Since the thermal conductivity and the cross section are considerably lower than those of YAG the material has not found applications.

Fluorides

The divalent fluorides are relatively soft, isotropic crystals. Rare earth-doped CaF_2 crystals have been studied extensively [2.23, 24], since this material was the host of many early solid-state lasers.

Doping of fluorides with trivalent rare earth ions requires charge compensation which complicates the crystal growth process. The important representative of this crystal family is yttrium lithium fluoride ($YLiF_4$), a uniaxial crystal. $YLiF_4$ is transparent to 150 nm. Therefore, high-current-density xenon flashlamps which emit strongly in the blue and near-ultraviolet can be used as pump sources without damage to the material. The most common dopant of YLF is Nd^{3+}. Nd:YLF offers a reduction in thermal lensing and birefringence combined with improved energy storage relative to Nd:YAG. The thermomechanical properties of Nd:YLF, however, are not as good as those of Nd:YAG. Details of Nd:YLF are discussd in Sect. 2.3.4.

Ceramics

In recent years, polycrystalline Nd:YAG ceramics have been produced with good optical quality. Lasers that have incorporated a Nd:YAG ceramic as active element have achieved power outputs and efficiencies comparable to single crystal Nd:YAG lasers [2.25–27]. Previously, transparent Nd:doped ceramics were plagued with high-scattering losses. Improved fabrication methods in the ceramic formation and sintering process have led to polycrystalline materials with very narrow grain boundaries and a very low porosity. These new highly transparent Nd:YAG ceramics are characterized by a very low-scattering loss.

Compared to Nd:YAG single crystals, Nd:YAG ceramics can be produced with higher Nd concentration and larger size. Nd:YAG ceramics are promising candidates for microchip lasers because they combine the advantage of Nd:YAG and Nd:YVO_4, which are the two leading materials for these applications. Ceramics can be highly doped for efficient pump absorption similar to Nd:YVO_4, and the material has the conductivity of Nd:YAG, which is twice as high as that of Nd:YVO_4.

2.1.2 Active Ions

Before proceeding to a discussion of the active laser ions, we will review briefly the nomenclature of atomic energy levels.

Different energy states of electrons are expressed by different quantum numbers. The electrons in an atom are characterized by a principal quantum number n, an orbital angular momentum l, the orientation of the angular momentum vector m, and a spin quantum number s. A tradition from the early days of line series allocation has established the following method of designating individual electronic orbits: a number followed by a letter symbolizes the principal quantum number n and the angular momentum number l, respectively. The letters s, p, d, f stand for $l = 0, 1, 2, 3$, respectively. For example, a 3d electron is in an orbit with $n = 3$ and $l = 2$.

To designate an atomic energy term one uses by convention capital letters with a system of subscripts and superscripts. The symbol characterizing the term is of the form $^{2S+1}L_J$, where the orbital quantum numbers $L = 0, 1, 2, 3, 4, 5$, are expressed by the capital letters S, P, D, F, G, H, I. A superscript to the left of the letter indicates the value $(2S + 1)$, that is, the multiplicity of the term due to possible orientation of the resultant spin S. Thus a one-electron system ($S = 1/2$) has a multiplicity 2. L and S can combine to a total angular momentum J, indicated by a subscript to the right of the letter. Thus the symbol $^2P_{3/2}$ shows an energy level with an orbital quantum number $L = 1$, a spin of $S = 1/2$, and a total angular momentum of $J = 3/2$. The complete term description must include the configuration of the excited electron, which precedes the letter symbol. Thus the ground state of lithium has the symbol $2s\ ^2S_{1/2}$.

When an atom contains many electrons, the electrons that form a closed shell may be disregarded and the energy differences associated with transitions in the atom may be calculated by considering only the electrons outside the closed shell.

In describing the state of a multielectron atom, the orbital angular momenta and the spin angular momenta are added separately. The sum of the orbital angular momenta are designated by the letter L, and the total spin is characterized by S. The total angular momentum J of the atom may then be obtained by vector addition of L and S. The collection of energy states with common values of J, L, and S is called a term.

In the following section, a qualitative description is given of some of the prominent features of the most important rare earth, actinide, and transition metal ions.

Rare Earth Ions

The rare earth ions are natural candidates to serve as active ions in solid-state laser materials because they exhibit a wealth of sharp fluorescent transitions representing almost every region of the visible and near-infrared portions of the electromagnetic spectrum. It is a characteristic of these lines that they are very sharp, even in the presence of the strong local fields of crystals, as a result of the shielding effect of the outer electrons.

The ground-state electronic configuration of the rare earth atom consists of a core which is identical to xenon, plus additional electrons in higher orbits. In xenon, the shells with quantum numbers $n = 1, 2, 3$ are completely filled. The shell $n = 4$ has its s, p, and d subshells filled, whereas the 4f subshell capable of accommodating 14 electrons is completely empty. However, the $n = 5$ shell has acquired its first 8 electrons which fill the 5s and 5p orbits. The electronic configuration for xenon is

$$1s^2 2s^2 2p^6 3s^2 3p^6 3d^{10} 4s^2 4p^6 4d^{10} 5s^2 5p^6.$$

Elements beyond xenon, which has the atomic number 54, have this electronic structure and, in addition, have electrons in the 4f, 5d, 6s, etc., orbits. Cesium, barium, and lanthanum are the elements between xenon and the rare earths. Cs has one, Ba has two 6s electrons, and La has in addition one electron in the 5d orbit. Rare earth

Table 2.1. Electronic configuration of trivalent rare earths

Element number	Trivalent rare earth	Number of 4f electrons	Ground state
58	Cerium, Ce^{3+}	1	$^2F_{5/2}$
59	Praseodymium, Pr^{3+}	2	$^3H_4$
60	Neodymium, Nd^{3+}	3	$^4I_{9/2}$
61	Promethium, Pm^{3+}	4	$^5I_4$
62	Samarium, Sm^{3+}	5	$^6H_{5/2}$
63	Europium, Eu^{3+}	6	$^7F_0$
64	Gadolinium, Gd^{3+}	7	$^8S_{7/2}$
65	Terbium, Tb^{3+}	8	$^7F_6$
66	Dysprosium, Dy^{3+}	9	$^6H_{15/2}$
67	Holmium, Ho^{3+}	10	$^5I_8$
68	Erbium, Er^{3+}	11	$^4I_{15/2}$
69	Thulium, Tm^{3+}	12	$^3H_6$
70	Ytterbium, Yb^{3+}	13	$^2F_{7/2}$
71	Lutetium, Lu^{3+}	14	$^1S_0$

elements begin with the filling of the inner vacant 4f orbits. For example, the first rare earth element cerium has only one electron in the f orbit:

$$\mathrm{Ce}: \ldots 4f5s^2 5p^6 5d6s^2,$$

and the important rare earth neodymium has four electrons in the f orbit

$$\mathrm{Nd}: \ldots 4f^4 5s^2 5p^6 6s^2.$$

Since the first nine shells and subshells up to $4d^{10}$ are completely filled, only the outer electron configuration is indicated.

In crystals, rare earth ions are normally trivalent, but under appropriate conditions the valence state can also be divalent. When a trivalent ion is formed the atom gives up its outermost 6s electrons; the atom loses also its 5d electron if it has one, otherwise one of the 4f electrons is lost. For example, trivalent Ce has the electronic configuration

$$\mathrm{Ce}^{3+}: \ldots 4f5s^2 5p^6$$

and trivalent Nd has the configuration

$$\mathrm{Nd}^{3+}: \ldots 4f^3 5s^2 5p^6 \ .$$

As one can see, the trivalent ions of rare earths have a simpler configuration than the corresponding atoms. Ions from the rare earths differ in electronic structure only by the number of electrons in the 4f shell as illustrated in Table 2.1. When a divalent rare earth ion is formed, the atom gives up its outermost 6s electrons.

The fluorescence spectra of rare earth ions arise from electronic transitions between levels of the partially filled 4f shell. Electrons present in the 4f shell can be raised by light absorption into unoccupied 4f levels. The 4f states are well shielded by the filled 5s and 5p outer shells. As a result, emission lines are relatively narrow and the energy level structure varies only slightly from one host to another. The

effect of the crystal field is normally treated as a perturbation on the free-ion levels. The perturbation is small compared to spinorbit and electrostatic interactions among the 4f electrons. The primary change in the energy levels is a splitting of each of the free-ion levels in many closely spaced levels as a result of the Stark effect of the crystal field. In crystals the free-ion levels are then referred to as manifolds. Figure 2.2 provides a nice illustration of the splitting of the Nd^{3+} manifolds into sublevels as a result of the YAG crystal field.

Neodymium. Nd^{3+} was the first of the trivalent rare earth ions to be used in a laser, and it remains by far the most important element in this group. Stimulated emission has been obtained with this ion incorporated in at least 100 different host materials, and a higher power level has been obtained from Nd lasers than from any other four-level material. The principal host materials are YAG and glass. In these hosts, stimulated emission is obtained at a number of frequencies within three different groups of transitions centered at 0.9, 1.06, and 1.35 μm. Radiation at these wavelengths results from $^4F_{3/2} \rightarrow {}^4I_{9/2}$, $^4I_{11/2}$, $^4I_{13/2}$ transitions, respectively.

The nomenclature of the energy levels may be illustrated by a discussion of the Nd^{3+} ion. This ion has three electrons in the 4f subshell. In the ground state their orbits are so aligned that the orbital angular momentum adds up to $3 + 2 + 1 = 6$ atomic units. The total angular momentum $L = 6$ is expressed by the letter I. The spins of the three electrons are aligned parallel to each other, providing an additional $3/2$ units of angular momentum, which, when added antiparallel to the orbital angular momentum, gives a total angular momentum of $6 - 3/2 = 9/2$ units. According to the quantum rules for the addition of angular momenta, the vector sum of an orbital angular momentum of 6 and a spin angular momentum of $3/2$ may result in the following four values of the total angular momentum: $9/2$, $11/2$, $13/2$, and $15/2$. The levels corresponding to these values are $^4I_{9/2}$, $^4I_{11/2}$, $^4I_{13/2}$, and $^4I_{15/2}$. The first of these, which has the lowest energy, is the ground state; the others are among the first few excited levels of Nd^{3+}. These levels are distinguished by the orientation of the spins with respect to the resultant orbital angular momentum. Other excited levels are obtained when another combination of the orbital angular momenta is chosen.

The most important Nd laser materials are described in Sect. 2.3.

Erbium. Laser action in erbium has been demonstrated in a variety of garnets, fluorides, and glasses. Erbium laser performance is not very impressive in terms of efficiency or energy output. However, erbium has attracted attention because of two particular wavelengths of interest. A crystal such as YAG highly doped with erbium produces an output around 2.9 μm, and erbium-doped phosphate glass generates an output at 1.54 μm (see Sect. 2.4). Both of these wavelengths are absorbed by water, which leads to interesting medical applications in the case of the 2.9 μm lasers and to eye safe military rangefinders in the case of the shorter wavelength.

The wavelength at 1.54 μm arises from a transition between the $^4I_{13/2}$ state and the $^4I_{15/2}$ ground state of Er^{3+}. At room temperature all levels of the terminal $^4I_{15/2}$ manifold are populated to some degree; thus, this transition forms a three-level laser scheme with a correspondingly high threshold.

The wavelength at 2.9 μm stems from a laser transition from the $^4I_{11/2}$ to the $^4I_{13/2}$ state. The lower laser level of this transition is considerably above the ground state, similar to the 1.06 μm transition in Nd^{3+}. Therefore this transition is four level in nature. However, complicated energy transfer mechanisms between the levels and a lower laser level which has a longer lifetime compared to the upper laser level has prevented cw operation at this transition.

Holmium. Laser action in Ho^{3+} has been reported in many different host materials [2.28]. Because the terminal level is only about 250 cm^{-1} above ground level, the lower laser level has a relatively high thermal population at room temperature. While Ho:YAG and Ho:YLF have proven to be efficient lasers, operation has been limited in most cases to cryogenic temperatures, which will depopulate the lower laser level. Previous efforts in flashlamp pumped 2 μm lasers have concentrated on Er:Tm:Ho doped YAG and YLF.

It was discovered that Cr-sensitized Tm:Ho:YAG offers several advantages over the Er-sensitized materials. In a Cr:Tm:Ho:YAG laser, a very efficient energy transfer process between the co-dopants takes place. Cr^{3+} acts to efficiently absorb flashlamp energy, which is then transferred to Tm with a transfer quantum efficiency approaching 2 (two photons in the IR for each pump photon). From Tm the energy is efficiently transferred to Ho. Lasing occurs at the $^5I_7$–$^5I_8$ Ho transition at a wavelength of 2080 nm [2.29]. Laser diode pumping of a Tm:Ho:YAG laser via an absorption line in Tm^{3+} at 780 nm is also possible [2.30]. Chromium doping is not necessary in this case (see also Sect. 2.5.4).

Thulium. Efficient flashlamp and laser diode-pumped laser operation has been achieved in Tm^{3+}:YAG and Tm^{3+}:YLF codoped either with Cr^{3+} or Ho^{3+}. The output wavelength for the $^3F_4$–$^3H_6$ transition is 2.01 μm. The thulium ion has an absorption at 785 nm, which is useful for diode pumping. With diode pumping Tm:YAG lasers have been designed with output powers in excess of 100 W. Cr doping provides for efficient absorption of the flashlamp radiation. Flashlamp-pumped Cr:Tm:YAG can achieve tunable output between 1.945 and 1.965 μm.

Thulium- and thulium-sensitized holmium lasers have outputs in the 2 μm region, a wavelength of interest for coherent radar systems, remote sensing, and medical applications. The possibility of pumping thulium-doped crystals, with readily available powerful GaAlAs laser diodes at 785 nm, has stimulated interest in these materials. Energy transfer and other relevant spectroscopic data of the Tm:YAG laser are covered in Sect. 2.5.4.

Praseodymium, Gadolinium, Europium, Ytterbium, Cerium. Laser action in all these triply ionized rare earths has been reported; however, only marginal performance was obtained in hosts containing these ions with the exception of ytterbium. Diode-pumped Yb:YAG has become an important laser and is described in Sect. 2.6.

Recently another Yb-doped crystal, namely Yb:KGW which is yttrium tungstate, KGd $(WO_4)_2$ has found applications in mode locked lasers. This crystal has a high

emission cross section, broad emission spectrum from 1020 to 1060 nm, and can be pumped with diode lasers at 940 or 980 nm. Diode-pumped Yb:KGW lasers have been developed for the generation of femto second pulses at an output wavelength of 1048 nm.

Samarium, Dysprosium, Thulium. The divalent rare earths Sm^{2+}, Dy^{2+}, and Tm^{2+} have an additional electron in the 4f shell, which lowers the energy of the 5d configuration. Consequently, the allowed 4f–5d absorption bands fall in the visible region of the spectrum. These bands are particularly suitable for pumping the laser systems. Tm^{2+}, Dy^{2+}, and Sm^{2+} have been operated as lasers, all in a CaF_2 host. For laser operation, these crystals must be refrigerated to at least 77 K.

Actinide Ions

The actinides are similar to the rare earths in having the 5f electrons partially shielded by 6s and 6p electrons. Most of the actinide elements are radioactive, and only uranium in CaF_2 has been successfully used in a laser [2.24]. The host was doped with 0.05% uranium. Laser action occurred at 2.6 μm between a metastable level and a terminal level some 515 cm^{-1} above the ground state.

Transition Metals

Important members of the transition-metal group include chromium and titanium. The chromium atom has 18 electrons in orbitals which make up the filled core. The outer configuration includes six electron in the d and s orbitals:

$$Cr: \ldots 3d^5 4s.$$

The trivalent chromium ion has given up three electrons from these outer two sets of orbitals

$$Cr^{3+}: \ldots 3d^3,$$

leaving three electrons in the 3d orbitals. These electrons determine the optical properties of the ion. Since they are unshielded by outer shells of electrons, in contrast to rare earth ions, the optical properties of transition-metal ions are strongly influenced by the host crystal field.

The titanium atom has the same electronic configuration as chromium, but only four electrons in the d and s orbitals:

$$Ti: \ldots 3d^2 4s^2.$$

The trivalent titanium has only a single electron in the d orbital:

$$Ti^{3+}: \ldots 3d.$$

Transition metal/host crystal combinations that have resulted in important lasers include ruby (Cr^{3+}:Al_2O_3), alexandrite (Cr^{3+}:$BeAl_2O_4$), Cr^{3+}:LiSAF

(Cr^{3+}:$LiSrAlF_6$), and Ti-sapphire (Ti^{3+}:Al_2O_3) lasers, which are discussed in separate sections.

In addition, Cr:forsterite (Cr^{4+}:Mg_2SiO_4) need to be mentioned because this laser is employed in the generation of femtosecond pulses. Both pulsed and cw laser operation has been achieved in Cr^{4+}:Mg_2SiO_4 with Nd:YAG lasers at 1.06 μm and 532 nm as pump sources. The tuning range covers the spectral region from 1167 to 1345 nm. A distinguishing feature of laser actions in Cr^{+}:Mg_2SiO_4 is that the lasing ion is not trivalent chromium (Cr^{3+}) as in the case with other chromium-based lasers, but the active ion in this crystal is tetravalent chromium (Cr^{4+}) which substitutes for silicon (Si^{4+}) in a tetradedral site.

Several other transition-metal-based lasers that have been offered commercially at one time or another include Cr:GSGG, Cr:$KZnF_3$, and Co:MgF_2. We will briefly come back to these lasers in Sect. 2.5.

2.2 Ruby

The ruby laser, Cr^{3+}:Al_2O_3, is a three-level system, which makes it necessary to pump the crystal at high intensity to achieve at least inversion. Consequently, the overall system efficiency is very low, which is the main reason for its limited use today. Ruby chemically consists of sapphire (Al_2O_3) in which a small percentage of the Al^{3+} has been replaced by Cr^{3+}. This is done by adding small amounts of Cr_2O_3 to the melt of highly purified Al_2O_3. Sapphire has the best thermomechanical properties of all solid-state laser materials. The crystal is very hard, has high thermal conductivity, and can be grown to very high quality by the Czochralski method. The Cr^{3+} ion has three d electrons in its unfilled shell; the ground state of the free ion is described by the spectroscopic symbol ^{4}A. The amount of doping is nominally 0.05 wt.% Cr_2O_3.

A simplified energy level diagram of ruby is shown in Fig. 2.1. In ruby lasers, population inversion with respect to the ^{2}E level is obtained by optically pumping Cr^{3+} ions from the $^4A_2$ ground state to the broad pump bands $^4T_2$ and $^4T_1$. The lifetime at the pump bands, which are each about 1000-nm wide, located in the green (18,000 cm^{-1}) and in the violet (25,000 cm^{-1}), is extremely short, with the ions returning to a metastable state ^{2}E that has a fluorescent life-time of 3 ms. This metastable level is split into two sublevels with a separation of $\Delta E = 29\,cm^{-1}$. The upper sublevel is the $2\bar{A}$ and the lower one the $\bar{E}$ sublevel. The two transitions ($\bar{E} \rightarrow {}^4\bar{A}_2$ and $2\bar{A} \rightarrow {}^4A_2$) are referred to as the R_1 and R_2 lines, which are located at the end of the visible region at 594.3 and 692.9 nm, respectively. The width of these fluorescent lines is $\Delta\nu = 330\,GHz$ at room temperature and they are homogeneously broadened because of the interaction of the Cr^{3+} ions with lattice vibrations. The two R lines are connected to each other by a very fast nonradiative decay; thermalization of the population occurs, and this results in the lower-lying $\bar{E}$ level being the more heavily populated.

At thermal equilibrium the difference in population between the $\bar{E}$ and $2\bar{A}$ level is determined by the Boltzmann factor $\kappa = \exp(\Delta E/kT)$. At room temperature the Boltzmann factor is $\kappa = 0.87$. The R_1 line attains laser threshold before the R_2 line

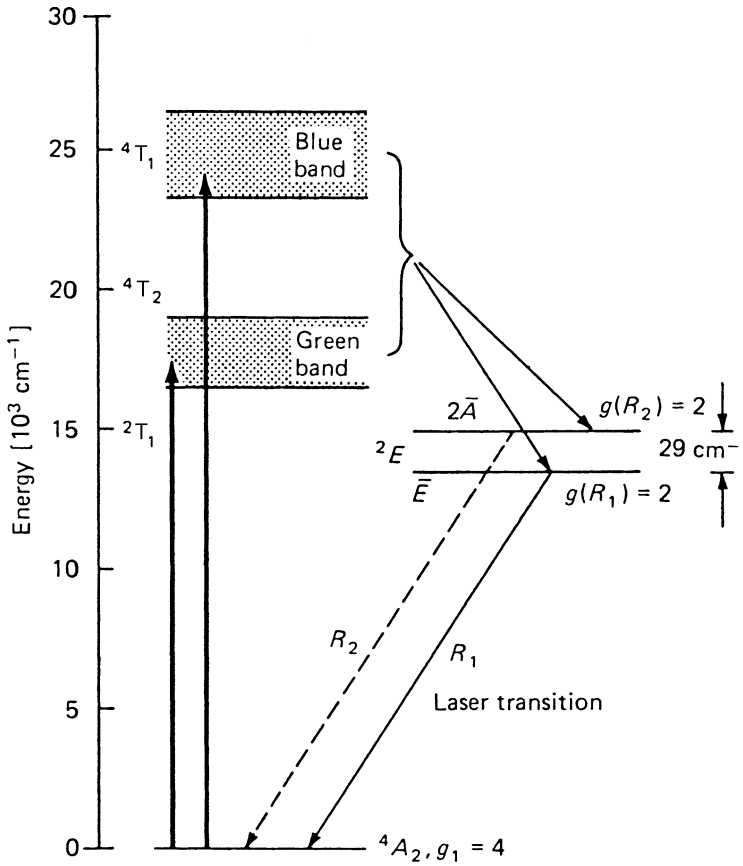


Fig. 2.1. Important energy levels of Cr^{3+} in ruby (separation of 2E levels not to scale)

because of the higher inversion. Once laser action commences in the R_1 line, the $\bar{E}$ level becomes depleted and population transfer from the nearby $2\bar{A}$ level proceeds at such a fast rate that the threshold level is never reached for the R_2 line. Therefore, the entire initial population of the two states decays through R_1 emission. If we compare the energy-level diagram of ruby with our simplified scheme of a three-level system in Fig. 1.6, the levels $^4T_1$ and $^4T_2$ jointly constitute level 3, whereas ^2E and $^4\bar{A}_2$ states represent levels 2 and 1, respectively. We can write

$$n_2 = n_2(R_1) + n_2(R_2) \tag{2.1}$$

for the metastable level and n_1 for the ground level. Threshold and gain in ruby depends only on the population of level $n_2(R_1)$. However, in relating gain and threshold to the population of the ground level n_1 or to the total number of Cr^{3+} ions n_{tot}, one has to take the population of $n_2(R_2)$ into account. In ruby all levels are degenerate, that is,

$$g(n_1) = 4, \qquad g(R_1) = g(R_2) = 2. \tag{2.2}$$

Because of the higher degeneracy of the ground state, amplification occurs when the R_1 level is at least one-half as densely populated as the ground state. Since

$$n_2(R_1) + n_2(R_2) + n_1 = n_{\text{tot}}, \tag{2.3}$$

we have the following population at threshold (300 K)

$$\begin{aligned} n_2(R_1) &= \frac{n_{\text{tot}}}{3+\kappa} = 0.26 n_{\text{tot}}, \\ n_2(R_2) &= \frac{\kappa n_{\text{tot}}}{3+\kappa} = 0.22 n_{\text{tot}}, \\ n_1 &= \frac{2n_{\text{tot}}}{3+\kappa} = 0.52 n_{\text{tot}}. \end{aligned} \tag{2.4}$$

Thus we must have just under one-half of the atoms in the two upper levels in order to reach threshold. With a Cr^{3+} concentration of $n_{\text{tot}} = 1.58 \times 10^{19}$ cm^{-3} and a photon energy of $h\nu = 2.86 \times 10^{-19}$ W s, we obtain for the energy density at the metastable level required to achieve transparency in ruby according to (2.4),

$$J_{\text{th}} = \left(\frac{\kappa+1}{\kappa+3}\right) n_{\text{tot}} h\nu = 2.18 \text{ J/cm}^3. \tag{2.5}$$

The small-signal gain coefficient in ruby is

$$g_0 = \sigma \left[n_2(R_1) - \frac{g(R_1) n_1}{g(n_1)} \right], \tag{2.6}$$

where σ is the stimulated emission cross section of the R_1 line and $n_2(R_1)$ is the population density of the E level.

Since $\sigma = \sigma_{12} g(n_1)/g(R_1)$, the gain coefficient can be expressed as (assuming $\kappa = 1$)

$$g_0 = \alpha_0 \left(\frac{2n_2}{n_{\text{tot}}} - 1 \right), \tag{2.7}$$

where $\alpha_0 = \sigma_{12} n_{\text{tot}}$ is the absorption coefficient of ruby. Ruby has an absorption cross section of $\sigma_{12} = 1.22 \times 10^{-10}$ cm^2 and an absorption coefficient of $\alpha_0 = 0.2$ cm^{-1}. With all the chromium ions in the ground state ($n_2 = 0$), the gain of the unpumped ruby crystal is $g_0 = -\alpha_0$. With all the ions in the upper levels ($n_2 = n_{\text{tot}}$), the maximum gain coefficent is $g_0 = \alpha_0$. (with the approximation $\kappa = 1$)

The example of ruby illustrates very clearly the drawbacks of a three-level system.

(a) Compared to a four-level laser, three-level lasers such as ruby and Er:glass, and quasi-three-level lasers such as Yb:YAG require high-pump intensities because a certain amount of pump power is required just to achieve transparency in the material.
(b) Since three-level and quasi-three-level lasers absorb at the laser wavelenght unless pumped to inversion, any portion of the laser crystal which is shielded from the pump light, for example, by the rod holder, will present a hight absorption loss.

Despite these obvoius drawbacks, three-level lasers have other redeeming features, such as desirable wavelenght or a particular efficient pump method, which makes these lasers attractive. For example, the ruby laser emits in the visible region, has broad absorption bands at a wavelength region particularly well-suited for flashlamp pumping, and has a long fluorescent lifetime and a reasonably large stimulated emission cross section.

2.3 Nd:Lasers

From the large number of Nd:doped materials, the lasers discussed in more detail in this chapter have gained prominence. Nd:YAG, because of its high gain and good thermal and mechanical properties, is by far the most important solid-state laser for scientific, medical, industrial, and military applications. Nd:glass is important for laser fusion drivers because it can be produced in large sizes. Nd:Cr:GSGG has received attention because of the good spectral match between the flashlamp emission and the absorption of the Cr ions. An efficient energy transfer between the Cr and Nd ions results in a highly efficient Nd:laser. Nd:YLF is a good material for a number of applications, because the output is polarized, and the crystal exhibits low thermal birefringence. It has a higher energy storage capability (due to its low gain coefficient) compared to Nd:YAG and its output wavelength matches that of phosphate Nd:glass, therefore modelocked and Q-switched Nd:YLF lasers have become the standard oscillators for large glass lasers employed in fusion research. Nd:YVO_4 has become a very attractive material for small diode-pumped lasers because of its large emission cross section and strong absorption at 809 nm.

2.3.1 Nd:YAG

The Nd:YAG laser is by far the most commonly used solid-state laser. Neodymium-doped yttrium aluminum garnet (Nd:YAG) possesses a combination of properties uniquely favorable for laser operation. The YAG host is hard, of good optical quality, and has a high thermal conductivity. Furthermore, the cubic structure of YAG favors a narrow fluorescent linewidth, which results in high gain and low threshold for laser operation. In Nd:YAG, trivalent neodymium substitutes for trivalent yttrium, so charge compensation is not required.

Physical Properties

In addition to the very favorable spectral and lasing characteristics displayed by Nd:YAG, the host lattice is noteworthy for its unusually attractive blend of physical, chemical, and mechanical properties. The YAG structure is stable from the lowest temperatures up to the melting point, and no transformations have been reported in the solid phase. The strength and hardness of YAG are lower than ruby but still high enough so that normal fabrication procedures do not produce any serious breakage problems.

Table 2.2. Physical and optical properties of Nd:YAG

Chemical formula	Nd:$Y_3Al_5O_{12}$
Weight % Nd	0.725
Atomic % Nd	1.0
Nd atoms/cm^3	1.38×10^{20}
Melting point	1970°C
Knoop hardness (kg/mm^2)	1320
Density	4.56 g/cm^3
Tensile strength	200 MPa
Modulus of elasticity	310 Gpa
Poisson ratio	0.30
Thermal expansion coefficient	
[100] orientation	8.2×10^{-6}/°C,
[110] orientation	7.7×10^{-6}/°C,
[111] orientation	7.8×10^{-6}/°C,
Linewidth	120 GHz
Stimulated emission cross section	
$R_2 - Y_3$	$\sigma = 6.5 \times 10^{-19}$ cm^2
$^4F_{3/2} - {}^4I_{11/2}$	$\sigma = 2.8 \times 10^{-19}$ cm^2
Fluorescence lifetime	230 μs
Photon energy at 1.06 μm	$h\nu = 1.86 \times 10^{-19}$ J
Index of refraction	1.82 (at 1.0 μm)

Pure $Y_3Al_5O_{12}$ is a colorless, optically isotropic crystal which possesses a cubic structure characteristic of garnets. In Nd:YAG about 1% of Y^{3+} is substituted by Nd^{3+}. The radii of the two rare earth ions differ by about 3%. Therefore, with the addition of large amounts of neodymium, strained crystals are obtained, indicating that either the solubility limit of neodymium is exceeded or that the lattice of YAG is seriously distorted by the inclusion of neodymium. Some of the important physical properties of YAG are listed in Table 2.2 together with optical and laser parameters [2.31–38]. Thermal properties of Nd:YAG are summarized in Table 2.3.

When operating a laser cw, or at a pulse repetition frequency higher than the inverse of the fluorescence lifetime, maintaining good extraction efficiency depends on having a beam intensity significantly larger than the saturation intensity $I_s = h\nu/\sigma\tau_f$, where $h\nu$ is the photon energy, σ is the emission cross section, and τ_f is the fluoresence lifetime. In low repetition rate pulsed systems the fluence in the resonator must be

Table 2.3. Thermal properties of Nd:YAG

Property	Units	300 K	200 K	100 K
Thermal conductivity	W cm^{-1} K^{-1}	0.14	0.21	0.58
Specific heat	W s g^{-1} K^{-1}	0.59	0.43	0.13
Thermal diffusivity	cm^2 s^{-1}	0.046	0.10	0.92
Thermal expansion	K^{-1} $\times 10^{-6}$	7.5	5.8	4.25
$\partial n/\partial T$	K^{-1}	7.3×10^{-6}	—	—

higher than the saturation fluence $J_s = h\nu/\sigma$. From the parameters listed in Table 2.2 it follows that for Nd:YAG a saturation intensity $I_s = 2.9$ kW/cm^2 and a saturation fluence $J_s = 0.67$ J/cm^2.

Laser Properties

Figure 2.2 depicts the energy level diagram of Nd:YAG. Stark splitting of the manifolds are shown on the right-hand side. Each of the $^{2S+1}L_J$ manifolds is split by the crystal field into $J + 1/2$ sublevels. The actual laser transitions occur between these individual Stark levels. The heavy line in Fig. 2.2 indicates the main laser transition in Nd:YAG having a wavelength of 1064 nm. The dashed lines represent transitions leading to 1.3 μm and 946 nm radiation.

The laser transition at 1064 nm occurs between the upper Stark level of the $^4F_{3/2}$ manifold (R_2 sublevel) and a Stark level within the $^4I_{11/2}$ manifold (Y_3 sublevel). At room temperature only 40% of the $^4F_{3/2}$ population is at level R_2; the remaining 60%

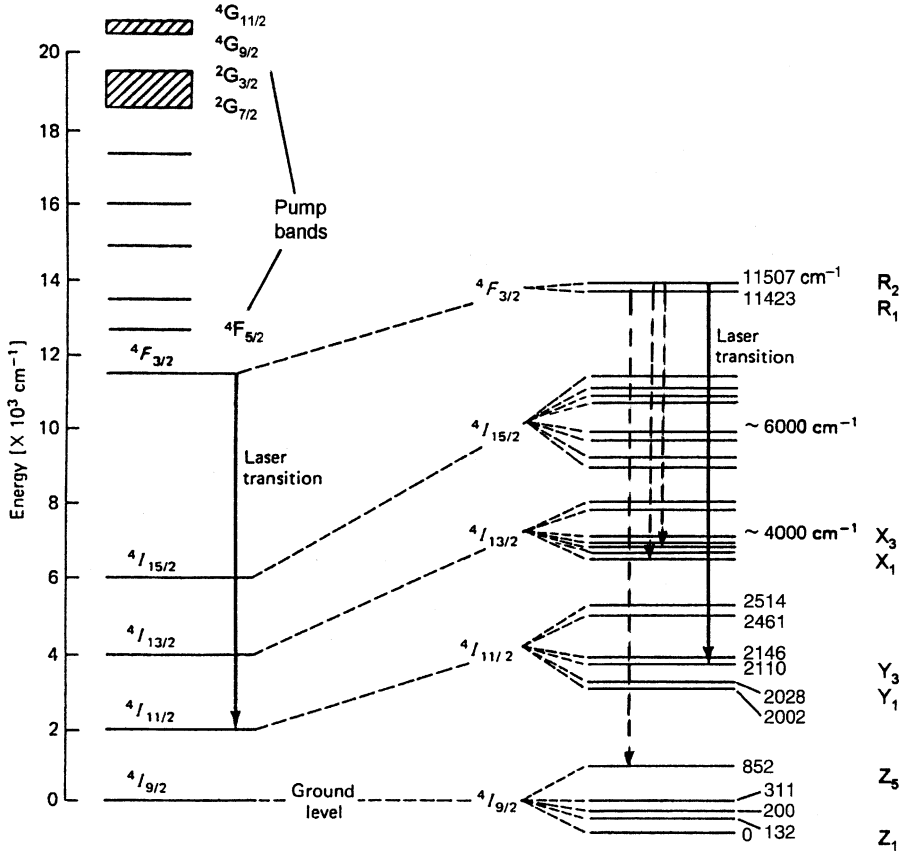


Fig. 2.2. Energy level diagram of Nd:YAG. The solid line represents the major transition at 1064 nm, and the dashed lines are the transitions at 1319, 1338, and 946 nm.

are at the lower sublevel R_1 according to Boltzmann's law. Lasing takes place only by R_2 ions whereby the R_2 level population is replenished from R_1 by thermal transitions. The ground level of Nd:YAG is the $^4I_{9/2}$ level. The terminal laser level is 2110 cm^{-1} above the ground state, and thus the population is a factor of $\exp(\Delta E/kT) \approx \exp(-10)$ of the ground-state density. Since the terminal level is not populated thermally, Nd:YAG is a four- level laser and the threshold condition is easy to obtain.

The fluorescence lifetime of the $^4F_{3/2}$ manifold is about 230 μs for Nd doping concentrations around 1% [2.38].

The branching ratios for room temperature fluorescence from the upper laser level to the various manifolds are as follows [2.5]: $^4F_{3/2} \rightarrow {}^4I_{9/2} = 0.30$, $^4F_{3/2} \rightarrow {}^4I_{11/2} = 0.56$, $^4F_{3/2} \rightarrow {}^4I_{13/2} = 0.14$, and $^4F_{3/2} \rightarrow {}^4I_{15/2} < 0.01$. The strongest fluorescence output is from the upper manifold to the lower manifold containing the laser transition at 1064 nm.

Above the upper laser level are located the pump bands starting with the manifold $^4F_{5/2}$, which is responsible for absorption around 808 nm. The highest laying manifold in Fig. 2.2 causes absorption in the visible region. Ions excited into these various pump bands relax efficiently to the upper laser level.

At room temperature the main 1.06 μm line in Nd:YAG is homogeneously broadened by thermally activated lattice vibrations. The spectroscopic cross section for the individual transition between Stark sublevels has been measured [2.33] to be $\sigma(R_2 - Y_3) = 6.5 \times 10^{-19} cm^2$. At a temperature of 295 K, the Maxwell–Boltzmann fraction in the upper Stark sublevel is 0.427, implying an effective cross section for Nd:YAG of $\sigma(^4F_{3/2} - {}^4I_{11/2}) = 2.8 \times 10^{-19} cm^2$. The effective stimulated-emission cross section is the spectroscopic cross section times the occupancy of the upper laser level relative to the entire $^4F_{3/2}$ manifold population.

Figure 2.3 shows the fluorescence spectrum of Nd^{3+} in YAG near the region or the laser output with the corresponding energy levels for the various transitions. The

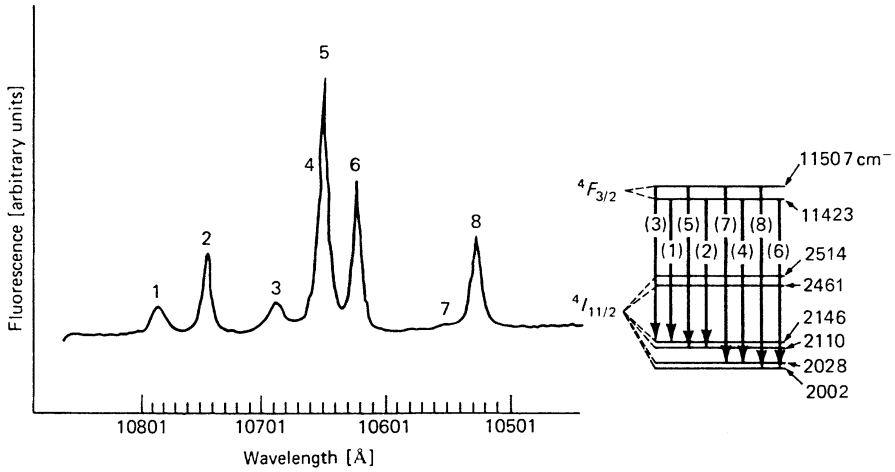
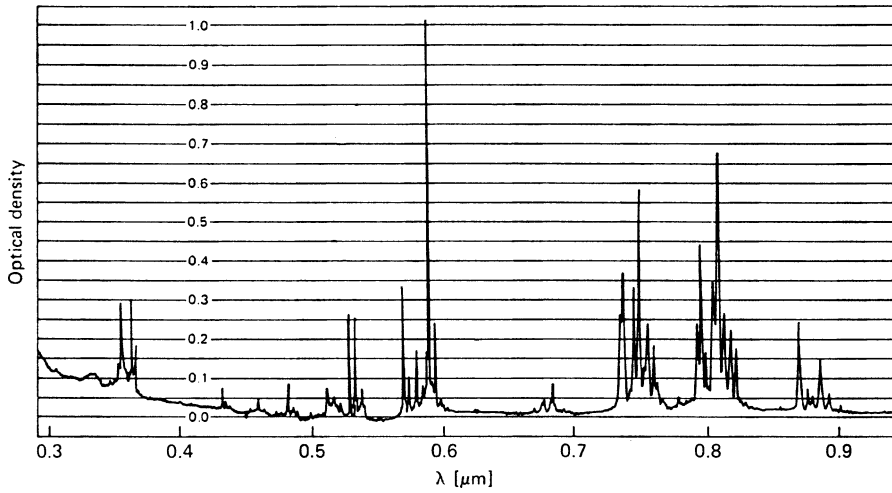
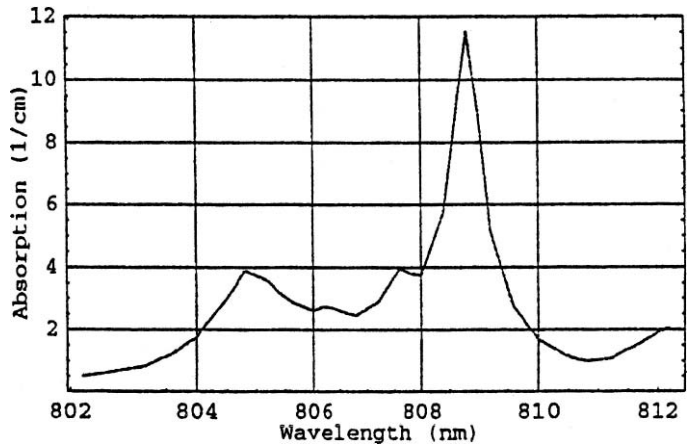


Fig. 2.3. Fluorescence spectrum of Nd^{3+} in YAG at 300 K in the region of 1.06 μm [2.10, 38].



(a)



(b)

Fig. 2.4. (a) Absorption spectrum of Nd:YAG from 0.3 to 0.9 μm and (b) expanded scale around 808 nm.

absorption of Nd:YAG in the range of 0.3–0.9 μm is shown in Fig. 2.4a. In Fig. 2.4b the absorption spectrum is expanded around the wavelength of 808 nm, which is important for laser diode pumping.

We can relate the absorption spectrum Fig. 2.4a to the energy level diagram in Fig. 2.2. The absorption peaks shown around 870 nm are caused by a transition from the ground level directly to the manifold containing the upper laser level $^4I_{9/2} \rightarrow {}^4F_{3/2}$. The absorption around 808 nm is the result of the $^4I_{9/2} \rightarrow {}^4F_{5/2}$ transition. The manifold $^4F_{5/2}$, comprising three Stark sublevels and located at about 12, 776 cm^{-1}, is the lowest pump band on the energy scale shown in Fig. 2.2. This is the main absorption

pump band for laser diode pumping at 808 nm. The absorption around 750 nm is the result of the manifold immediately above $^4F_{5/2}$. Both absorption regions around 810 and 750 nm are improtant for pumping Nd:YAG with cw arc lamps. The absorption peaks around 540 and 590 nm relate to the upper energy levels around 19,000 and 20,500 cm^{-1} shown in Fig. 2.2. The pump bands are important for flashlamp-pumped Nd:YAG lasers because flashlamps produce a large amount of radiation in the visible region.

Nd:YAG Laser Crystals

Commercially available laser crystals are grown exclusively by the Czochralski method. Growth rates, dopants, annealing procedures, and final size generally determine the manufacturing rate of each crystal. The boule axis or growth direction is customarily in the [111] direction. The high manufacturing costs of Nd:YAG are mainly due to the very slow growth rate of Nd:YAG, which is of the order of 0.5 mm/h. Typical boules of 10–15 cm in length require a growth run of several weeks.

Boules grown from Nd:YAG typically contain very few optically observable scattering centers and show negligible absorption at the lasing wavelength. However, all Nd:YAG crystals grown by Czochralski techniques show a bright core running along the length of the crystal when positioned between crossed polarizers. Strain flares are also visible, radiating from the core toward the surfaces of the crystal. Electron microprobe studies have revealed that in the core region the Nd concentration can run as much as twice as high as in the surrounding areas. The cores originate from the presence of facets on the growth interface which have a different distribution coefficient for neodymium than the surrounding growth surface. These compositional differences cause corresponding differences in thermal expansion coefficients which, in turn, give rise to the observed stress patterns during the cool down of the crystals from the growth temperature. Annealing does not seem to eliminate the cores and, thus far, no way has been found of avoiding the formation of facets on the growth interface. However, by choosing the growth direction carefully and by maintaining as steep an interface angle as is practical, the stresses can be confined to a very localized region and high-optical quality rods can be fabricated from the surrounding material. This means, of course, that in order to provide rods of a given diameter, the crystal must be grown with a diameter that is somewhat more than twice as large. The boules are processed by quartering into sections. Rods can be fabricated with maximum diameters of about 15 mm and lengths of up to 150 mm. The optical quality of such rods is normally quite good and comparable to the best quality of Czochralski ruby or optical glass. For example, 6 mm by 100 mm rods cut from the outer sections of 20 mm by 150 mm boules typically may show only 1–2 fringes in a Twyman–Green interferometer.

Neodymium concentration by atom percent in YAG has been limited to 1.0–1.5%. Higher doping levels tend to shorten the fluorescent lifetime, broaden the linewidth, and cause strain in the crystal, resulting in poor optical quality. The Nd doping level in YAG is sometimes expressed in different concentration units: A concentration

of 1.0% Nd atoms in the lattice is equivalent to 0.727% Nd or 0.848% Nd_2O_3 by weight, respectively. The concentration of Nd^{3+} sites in these cases is 1.386×10^{20} cm^{-3}.

In specifying Nd:YAG rods, the emphasis is on size, dimensional tolerance, doping level, and passive optical tests of rod quality. Cylindrical rods with flat ends are typically finished to the following specifications: end flat to $\lambda/10$, ends parallel to ± 4 arc seconds, perpendicularity to rod axis to ± 5 min, and rod axis parallel to within $\pm 5^\circ$ to [111] direction. Dimensional tolerances typically are ± 0.5 mm on length and ± 0.025 mm on diameter. Most suppliers furnish the laser crystals with a photograph showing the fringe pattern of the crystal as examined by a Twyman–Green interferometer. A double-pass Twyman–Green interferometer quickly reveals strained areas, small defects, or processing errors.

In a particular application the performance of a Nd:YAG laser can be somewhat improved by the choice of the optimum Nd concentration. As a general guideline, it can be said that a high-doping concentration (approximately 1.2%) is desirable for Q-switch operation because this will lead to high energy storage. For cw operation, a low-doping concentration (0.6–0.8%) is usually chosen to obtain good beam quality.

It is worth noting that in contrast to a liquid or a glass, a crystal host is not amenable to uniform dopant concentration. This problem arises as a result of the crystal-growth mechanism. In the substitution of the larger Nd^{3+} for a Y^{3+} in $Y_3Al_5O_{12}$, the neodymium is preferentially retained in the melt. The increase in the concentration of Nd from the seed to the terminus of a 20-cm long boule is about 20–25%. For a laser rod 3–8 cm long, this end-to-end variation may be 0.05–0.10% of Nd_2O_3 by weight.

Different Laser Transitions in Nd:YAG

Nd:YAG can produce other useful wavelength besides the familiar 1064 nm. From Fig. 2.2 it follows that there are 14, 12, and 10 transitions possible from the manifold $^4F_{3/2}$ to the $^4I_{13/2}$, $^4I_{11/2}$, $^4I_{9/2}$ manifolds respectively. The peak cross section and fluorescence branching ratios for fluorescence of these transitions are listed in [2.5]. Laser action has been achieved in many of these transitions [2.39–44].

In Nd:YAG the 1064 nm and 1061 nm transitions $^4F_{3/2} \rightarrow {}^4I_{11/2}$ have the highest emission cross sections. At room temperature the 1064 nm line $R_2 \rightarrow Y_3$ is dominant, while at low temperatures the 1061 line $R_1 \rightarrow Y_1$ has the lower threshold [2.45].

Several low-gain transitions, one at 946 nm and two at 1.3 μm, are of particular interest in Nd:YAG because frequency doubling of these wavelengths is attractive for producing powerful beams in the blue and red region of the spectrum. The transitions at 946 nm and at 1.3 μm are indicated by dashed lines in Fig. 2.2. Effective cross sections are listed in Table 2.4. To obtain output at these wavelengths, parasitic oscillations at the higher gain transitions are typically suppressed by dichroic mirrors and intracavity dispersive prisms.

There are two strong transitions in the 1.3 μm region from the $^4F_{3/2}$ to the $^4I_{13/2}$ manifold which have almost the same cross section and the laser output typically

Table 2.4. Important transitions in Nd:YAG [2.5, 7, 43]

Wavelength (nm)	Transition	Cross section (10^{-19} cm^2)
1064.1	$^4F_{3/2} \rightarrow {}^4I_{11/2}, (R_2 \rightarrow Y_3)$	2.8
1338.1	$^4F_{3/2} \rightarrow {}^4I_{13/2}, (R_2 \rightarrow X_3)$	1.0
1318.7	$^4F_{3/2} \rightarrow {}^4I_{13/2}, (R_2 \rightarrow X_1)$	0.95
946	$^4F_{3/2} \rightarrow {}^4I_{9/2}, (R_1 \rightarrow Z_5)$	0.5

contains both wavelength. One is the $R_2 \rightarrow X_1$ transition at 1319 nm and the other is the $R_2 \rightarrow X_3$ line at 1338 nm. Nd:YAG lasers that have been operated in this wavelength region are reported in [2.43, 46–49].

A flashlamp-pumped pulsed system achieved up to 165 W average power at 1.3 μm [2.46]. Intracavity doubling of a diode-pumped Nd:YAG laser operating at 1319 nm generated 6.1 W of cw red radiation at 659.5 nm. Efficiency and stability was improved by suppressing the 1338-nm line by inserting a thin etalon into the resonator [2.47]. With laser diode side pumping cw powers in excess of 100 W at 1319 nm have been reported [2.48].

The 946-nm emission originates from the R_1 Stark level of the $^4F_{3/2}$ manifold and terminates at the highest Stark level Z_5 of the ground manifold $^4I_{9/2}$. Because the lower laser level is only 852 cm^{-1} above the ground state, there is a thermal population of about 0.7% at room temperature. This residual population induces a partial reabsorption of the laser radiation which increases the threshold. Therefore, the laser operating at 946 nm emission is a quasi-three-level laser.

There is great interest in these transitions since frequency doubling of the 946 nm leads to the blue spectral region. An all solid-state blue laser could become an alternative to the argon-ion laser. Laser operating at 946 nm are reported in [2.44, 50–52]. Intracavity frequency doubling of a diode pumped system generated 4.6 W of output at 946 nm, which produced 2.8 W at the blue wavelength of 473 nm [2.52].

2.3.2 Nd:Glass

There are a number of characteristics that distinguish glass from other solid-state laser host materials. Its properties are isotropic. It can be doped at very high concentrations with excellent uniformity, and it can be made in large pieces of diffraction-limited optical quality. In addition, glass lasers have been made, in a variety of shapes and sizes, from fibers a few micrometers in diameter to rods 2 m long and 7.5 cm in diameter and disks up to 90 cm in diameter and 5 cm thick.

The most common commercial optical glasses are oxide glasses, principally silicates and phosphates, that is, SiO_2 and P_2O_5 based. Table 2.5 summarizes some important physical and optical properties of commercially available silicate and phosphate glasses.

Phosphate glasses have a larger emission cross section and a smaller nonlinear coefficient as compared to silicate glasses. These two attributes make Nd-doped

Table 2.5. Physical and optical properties of Nd-doped glasses

	Glass type					
Spectroscopic properties	Q–246 Silicate (Kigre)	Q–88 Phosphate (Kigre)	LHG–5 Phosphate (Hoya)	LHG–8 Phosphate (Hoya)	LG–670 Silicate (Schott)	LG–760 Phosphate (Schott)
Peak wavelength (nm)	1062	1054	1054	1054	1061	1054
Cross section ($\times 10^{-20}$ cm^2)	2.9	4.0	4.1	4.2	2.7	4.3
Fluorescence lifetime (μs)	340	330	290	315	330	330
Linewidth FWHM (nm)	27.7	21.9	18.6	20.1	27.8	19.5
Density (gm/cm^3)	2.55	2.71	2.68	2.83	2.54	2.60
Index of refraction (Nd)	1.568	1.545	1.539	1.528	1.561	1.503
Nonlinear coefficient (10^{-16} cm^2/W)	3.74	2.98	3.48	3.10	3.78	2.90
$dn/dt(20-40°C)$ ($10^{-6}/°C$)	2.9	−0.5	8.6	−5.3	2.9	−6.8
Thermal coefficient of optical path ($20-40°C$)($10^{-6}/°C$)	+8.0	+2.7	+4.6	+0.6	8.0	—
Transformation point (°C)	518	367	455	485	468	—
Thermal expansion coefficient ($20-40°C$)($10^{-7}/°C$)	90	104	86	127	92.6	138
Thermal conductivity (W/m °C)	1.30	0.84	1.19	—	1.35	0.67
Specific heat (J/g °C)	0.93	0.81	0.71	0.75	0.92	0.57
Knoop hardness	600	418	497	321	497	—
Young's modulus (kg/mm^2)	8570	7123	6910	5109	6249	—
Poisson's ratio	0.24	0.24	0.237	0.258	0.24	0.27

phosphate glasses the material of choice for large laser systems employed in fusion research [2.53–57].

There are two important differences between glass and crystal lasers. First, the thermal conductivity of glass is considerably lower than that of most crystal hosts. Second, the emission lines of ions in glasses are inherently broader than in crystals. A wider line increases the laser threshold. Nevertheless, this broadening has an advantage. A broader line offers the possibility of obtaining and amplifying shorter light pulses and, in addition, it permits the storage of larger amounts of energy in the amplifying medium for the same linear amplification coefficient. Thus, glass and crystalline lasers complement each other. For continuous or very high repetition-rate operation, crystalline materials provide higher gain and greater thermal conductivity. Glasses are more suitable for high-energy pulsed operation because of their large size, flexibility in their physical and optical parameters, and the broad fluorescent line width.

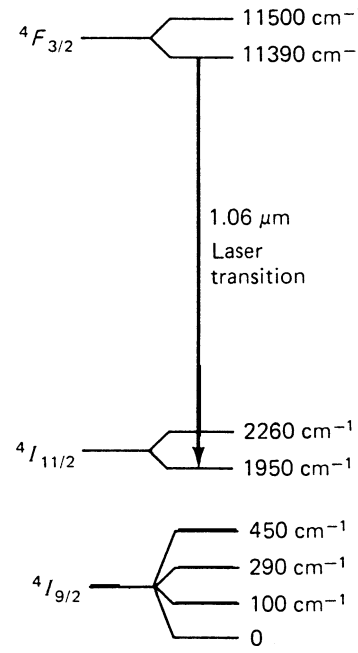


Fig. 2.5. Partial energy level diagram of Nd^{3+} in glass

Unlike many crystals, the concentration of the active ions can be very high in glass. The practical limit is determined by the fact that the fluorescence lifetime and, therefore the efficiency of stimulated emission, decreases with higher concentrations. In silicate glass, this decrease becomes noticeable at a concentration of 5% Nd_2O_3.

Figure 2.5 shows a simplified energy level diagram of Nd:glass. The Nd^{3+} ion in glass represents a four-level system. The upper laser level indicated in Fig. 2.5 is the lower-lying component of the $^4F_{3/2}$ pair with a several hundred microsecond spontaneous emission lifetime. The terminal laser level is the lower-lying level of the pair in the $^4I_{11/2}$ multiplet. The $^4I_{11/2}$ group empties spontaneously by a radiationless phonon transition to the $^4I_{9/2}$ ground state about 1950 cm^{-1} below.

Because of the large separation of the terminal laser level from the ground state even at elevated temperatures there is no significant terminal-state population and, therefore, no degradation of laser performance. In addition, the fluorescent linewidth of the neodymium ion in glass is quite insensitive to temperature variation; only a 10% reduction is observed in going from room temperature to liquid nitrogen temperature. As a result of these two characteristics, it is possible to operate a neodymium-doped glass laser with little change in performance over a temperature range of -100 to $+100$°C.

Figure 2.6 shows the pump bands of Nd:glass. In comparing Fig. 2.6 with Fig. 2.4, one notes that the locations of the absorption peaks in Nd:YAG and Nd:glass are about the same; however, in Nd:glass the peaks are much wider and have less fine a structure compared to Nd:YAG.

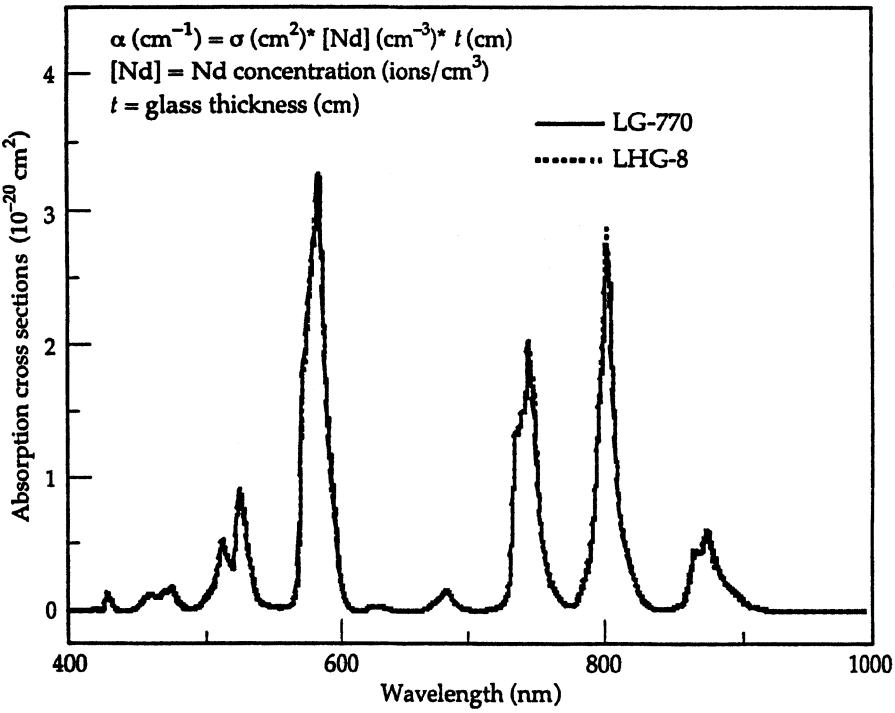


Fig. 2.6. Absorption spectra for two phosphate glasses [2.58]

Data Sources on Laser Glasses. Useful reviews on glass lasers can be found in [2.1, 2, 59, 60]. Pertinent materials parameters are listed in the data sheets of the major Nd:glass manufacturers.

2.3.3 Nd:Cr:GSGG

Soon after the invention of the Nd:YAG laser attempts were made to increase the absorption of pump radiation from flashlamps by incorporating a second dopant called a sensitizer into the laser crystal. A particularly attractive sensitizer is Cr^{3+} because the broad absorption bands of chromium can efficiently absorb light throughout the whole visible region of the spectrum. The concept of improving efficiency by co-doping a Nd laser crystal with Cr^{3+} ions is based on absorption of pump radiation by the broad absorption bands of Cr and nonradiative energy transfer to the Nd ions. No improvement was achieved with the host crystal YAG because of an inefficient transfer process. However, it was discovered [2.61,62] that a nearly 100% transfer efficiency could be achieved in the codoped garnet cyrstal GSGG. In Nd:Cr:YAG the $Cr^{3+} \rightarrow Nd^{3+}$ transfer time of 6.2 ms prevents the Cr^{3+} from being an effective sensitizer, because the transfer time has to be shorter than the 230 μs fluorescence decay time of Nd^{3+}. In Nd:Cr:GSGG the $Cr^{3+} \rightarrow Nd^{3+}$ transfer time has been measured to be

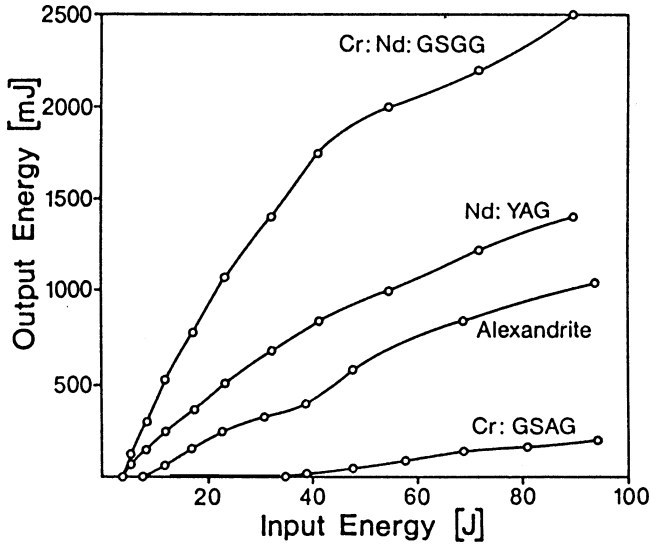


Fig. 2.7. Output energy versus input energy for Cr:Nd:GSGG, Nd:YAG, alexandrite, and Cr:GSAG [2.64]

17 μs [2.62]. This is due to a favorable red shift of the $^4T_1$ energy band of Cr^{3+}. It was found that the pumping efficiency improvement is not a strong function of the Cr concentration for the range of $1–2\times10^{20}/cm^3$ [2.63].

Figure 2.7 illustrates the high efficiency which can be achieved with this material by comparing it to Nd:YAG and to tunable lasers such as alexandrite and Cr:GSAG [2.64]. The experiments were carried out in a silver-plated single-ellipse pump cavity using a 5×75 mm^2 flashlamp. The laser rods were 6×75 mm^2 in an identical laser-resonator configuration but with output coupling optimized for the particular laser. The flashlamp pump efficiency of Nd:Cr:GSGG is about twice that of Nd:YAG.

The explanation for the high efficiency of codoped GSGG follows from Fig. 2.8, which shows the absorption spectrum of this material. Two high-intensity Cr^{+3} absorption bands having maxima at 450 and 640 nm covering an appreciable part of the visible region and narrow Nd lines can be observed.

The higher pump efficiency of Nd:Cr:GSGG does not automatically translate into better system performance because Nd:Cr:GSGG does exhibit much stronger thermal focusing and stress birefringence, as compared to Nd:YAG.

The crystal Nd:Cr:GSGG has a thermal conductivity that is about 2.5 times lower compared to Nd:YAG. Furthermore, the blue and red Cr absorption bands produce substantial quantum defect heating because of the large energy difference between pump and laser photons. As a consequence, thermal lensing is six to nine times more severe compared to Nd:YAG along with a three times greater thermally induced birefringence [2.66–68].

Therefore, if beam brightness is the criteria rather than output energy, the enhanced flashlamp pump efficiency advangtage of Nd:GSGG compared to Nd:YAG

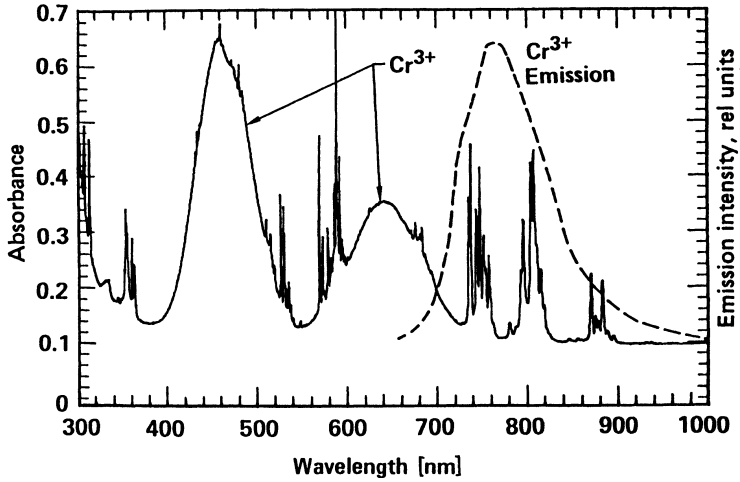


Fig. 2.8. Absorption spectra of Cr:Nd:GSGG [2.65]

is diminished because of larger thermally induced beam distortions. Measurements at the author's laboratory have shown that under single-shot and low-repetition-rate operation, beam brightness in a GSGG system is about twice as high as compared to YAG. However, as the repetition rate is increased, this difference became smaller and beam brightness for a given input was about equal in both systems at 25 Hz for a Q-switched system at 100 mJ output.

By incorporating advanced thermal lensing and birefringence compensation techniques, good beam quality and stable performance over a broad operating range was achieved from a Nd:Cr:GSGG laser [2.68]. The laser produced 150 mJ pulses at repetition rates of up to 20 Hz. Thermal lensing and astigmatism were corrected with a cylindrical telescope and an adjustable negative lens-rear mirror combination. Birefringence was partially compensated by adding a third resonator mirror and a Faraday rotator. This so-called reentrant resonator as well as the thermal lensing compensation technique are applicable to any solid-state laser and will be discussed further in Chap. 7.

2.3.4 Nd:YLF

The crystal Nd^{3+}:$LiYF_4$ has a number of attributes that offer an advantage over Nd:YAG in certain applications. The natural birefringence of this uniaxial crystal dominates thermally induced birefringence and the polarized output eliminates the thermal depolarization losses of optically isotropic hosts like YAG.

The transition of Nd:YLF at 1053 nm matches the peak gain of Nd-doped phosphate and fluorphosphate glasses. Since Nd:YLF can be cw pumped and mode-locked, a Nd:YLF oscillator provides a stable output for the selection of an individual short

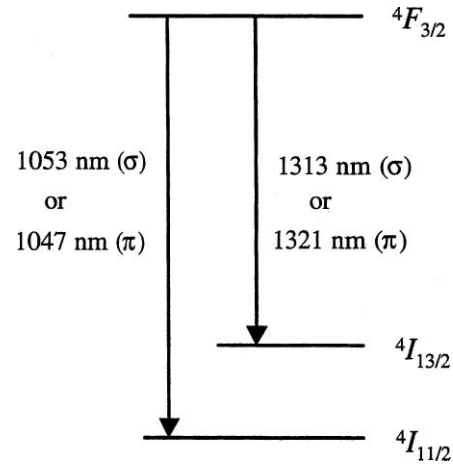


Fig. 2.9. Simplified energy level diagram of Nd:YLF

pulse. For this reason Nd:YLF is used in the master oscillators of Nd:glass amplifier chains.

The material also has advantages for diode pumping since the fluorescence lifetime in Nd:YLF is twice as long as in Nd:YAG. Laser diodes are power limited and, therefore a larger pump time afforded by the longer fluorescence time provides for twice the energy storage from the same number of diodes.

For laser diode pumping, Nd:YLF exhibits three absorption maxima, namely, at 792, 797, and 806 nm [2.69]. The largest absorption occurs at 792 nm, but the more powerful cw laser diodes are available at 806 nm. In some Nd:YLF lasers the pump wavelength of 797 nm is chosen as a compromise [2.70].

Fig. 2.9 shows a simplified energy level diagram of Nd:YLF. All lines originate on the same Stark split $^4F_{3/2}$ upper level. Depending on the polarization, two lines are obtained around 1.05 and 1.3 μm. The birefringence of Nd:YLF makes the gain of these lines a function of the laser polarization. For example, with an intracavity polarizer one can select either the 1047 nm (extraordinary beam) or the 1053 um (ordinary beam) transition. The same can be done for the two 1.3 μm transition; however, in addition lasing at the 1.05 μm lines has to be suppressed. The main reason for lasing Nd:YLF at one of the 1.3 μm transitions is for the production of red light [2.71, 72].

Material properties of Nd:YLF are listed in Table 2.6. Nd:YLF is a mechanically weaker and softer crystal compared to Nd:YAG with a lower thermal conductivity and emission cross section. Since the thermomechanical properties of Nd:YAG are far superior to those of Nd:YLF, the latter crystal is employed only in low- to medium-power systems.

For lasers requiring moderate Q-switch energies, the lower gain of Nd:YLF actually offers some advantages in system architecture over the high gain material Nd:YAG. The energy storage in Q-switched operation of Nd oscillators and amplifiers

Table 2.6. Properties of Nd-doped lithium yttrium fluoride (YLF)

Lasing wavelength (nm)	1053 (σ)
	1047 (π)
Index of refraction, $\lambda = 1.06\,\mu m$	$n_0 = 1.4481$
	$n_e = 1.4704$
Fluorescent lifetime	480 μs
Stimulated emission	$1.8 \times 10^{-19} (\pi)$
Cross section (cm^2)	$1.2 \times 10^{-19} (\sigma)$
Density (g/cm^3)	3.99 (undoped)
Hardness (Mohs)	4–5
Elastic modulus (N/m^2)	7.5×10^{10}
Strength (N/m^2)	3.3×10^7
Poisson's ratio	0.33
Thermal conductivity (W/(cm K))	0.06
Thermal expansion	*a* axis: 13×10^{-6}
coefficient ($^\circ C^{-1}$)	*c* axis: 8×10^{-6}
Melting point ($^\circ C$)	825

is constrained by the onset of parasitic oscillations. To first order, the energy storage limit of two materials is inversely proportional to the ratio of the stimulated emission cross sections. Therefore, higher storage densities are obtained in the lower cross section material Nd:YLF as compared to Nd:YAG.

Figure 2.10 shows the performance of a Q-switched YLF oscillator, producing an output of 400 mJ [2.73]. This output level would require the addition of an amplifier in the case of a Nd:YAG laser. Single oscillators with up to 0.5 J Q-switched output and oscillator-amplifier configurations with several Joules output usually result in less complicated structures if designed with Nd:YLF rods as compared to Nd:YAG [2.74, 75]. The weaker thermal lensing in Nd:YLF coupled with its natural

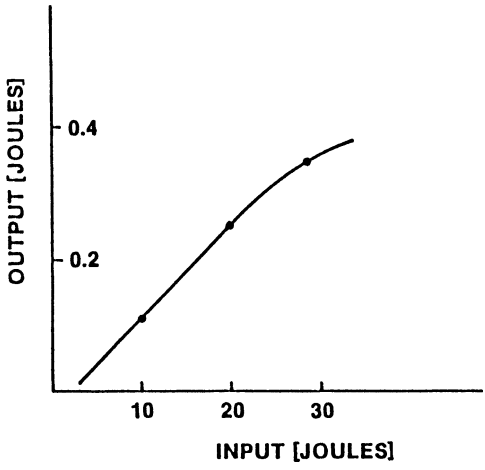


Fig. 2.10. Performance of a Q-switched YLF oscillator (laser rod: 0.25×2.5 $inch^2$; output coupler: 30% reflectivity; wavelength: 1.053 μm) [2.73]

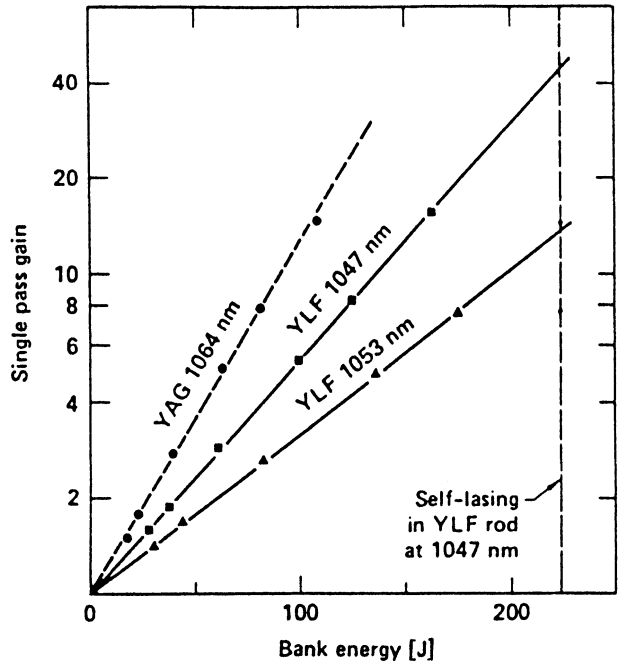


Fig. 2.11. Single-pass gain versus pump energy for YLF and YAG [2.74]

birefringence provide additional advantages in certain applications compared to Nd:YAG.

Figure 2.11 shows measured single-pass gain versus pump energy for the two transitions [2.74]. The measurements of the Nd:YLF amplifier were performed on a 10 mm diameter × 76 mm YLF rod with 1% Nd doping. The crystal was pumped in a silver-coated double elliptical pumping head. The YAG data were obtained by replacing the Nd:YLF with a 10 mm diameter Nd:YAG rod in the same amplifier head.

2.3.5 Nd:YVO_4

Neodymium-doped yttrium vanadate has several spectroscopic properties that are particularly relevant to laser diode pumping. The two outstanding features are a large stimulated emission cross section which is five times higher than Nd:YAG, and a strong broadband absorption at 809 nm.

The potential of Nd:YVO_4 as an important laser material has been recognized in 1966 [2.21]. However, crystals could not be grown free of scattering centers and absorbing color center defects. The unavailability of high-quality crystals of the size required for flashlamp pumping proved to be the major obstacle to further development. The high gain achievable in Nd:YVO_4 and the strong absorption of diode pump radiation require crystals only a few millimeters in length. With the constraint of large

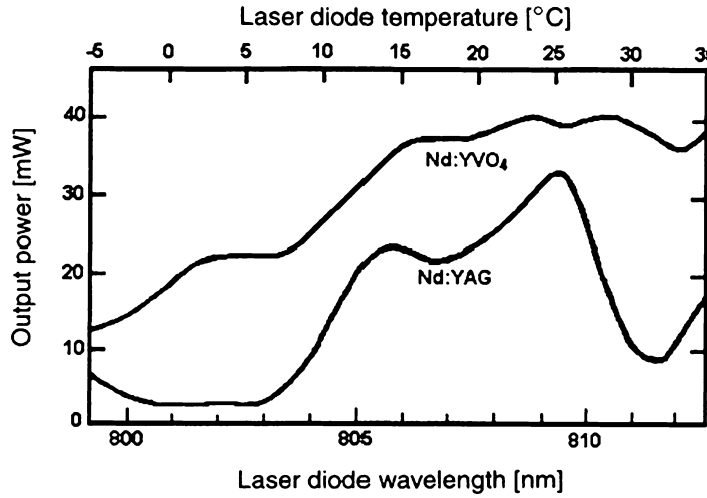


Fig. 2.12. Output from a Nd:YVO_4 and Nd:YAG laser as a function of diode pump temperature and wavelength [2.77]

crystal size removed, and with further improvements in the crystal growth process, material of high-optical quality became available.

The vanadate crystal is naturally birefringent and laser output is linearly polarized along the extraordinary π direction. The polarized output has the advantage that it avoids undesirable thermally induced birefringence.

Pump absorption in this uniaxial crystal is also polarization dependent. The strongest absorption occurs for pump light polarized in the same direction as the laser radiation. The absorption coefficient is about seven times higher compared to Nd:YAG in the π direction. The sublevels at the $^4F_{5/2}$ pump band are more resolved in Nd:YAG, whereas in Nd:YVO_4 Stark splitting is smaller and the multiple transitions are more compacted. The result is a broader and less spiky absorption profile of Nd:YVO_4 compared to Nd:YAG around the pump wavelength of 809 nm. Figure 2.12 gives an indication of the broader and smoother absorption profile of this material as compared to Nd:YAG. From this data follows also that Nd:YVO_4 laser performance is more tolerant to diode temperature variations because of the large pump bandwidth. If one defines this bandwidth as the wavelength range where at least 75% of the pump radiation is absorbed in a 5 mm thick crystal, then one obtains for Nd:YVO_4 a value of 15.7 nm and a value of 2.5 nm for Nd:YAG [2.78].

Table 2.7 summarizes important material parameters for Nd:YVO_4. The two outstanding features of this cyrstal, as already mentioned, are the high emission cross section and the large absorption coefficient for pump radiation at 809 nm. Major short comings of Nd:YVO_4 are a relatively low thermal conductivity and a short fluorescence lifetime.

The low thermal conductivity (about one-third that of Nd:YAG) prevents good heat dissipation, and the thermally induced fracture of the crystal raises a severe obstacle to scaling up to the operation to high power. This limitation can

Table 2.7. Material parameters for Nd:YVO_4 [2.78–80]

Laser cross section	15.6×10^{-19} cm^2
Laser wavelength	1064.3 nm
Linewidth	0.8 nm
Fluorescence lifetime	100 μs
Peak pump wavelength	808.5 nm
Peak absorption coefficient	34 (π polarization)
at 808 nm (cm^{-1})	10 (σ polarization)
Nd doping	1% (atomic Nd)
Modulus of elasticity	133 Gpa
Tensile strength	53 MPa
Thermal conductivity	0.05 W/cm K
Poisson ratio	0.33
Knoop hardness	480 kg/mm^2

be, to some extent, circumvented by using low-doped crystals as discussed further below.

As expressed in (3.65), the pump input power to reach threshold for cw operation is inversely proportional to the product of emission cross section σ and effective lifetime τ_f. The large cross section in Nd:YVO_4 is partially offset by its shorter lifetime. However, the product ($\sigma\,\tau_f$) is still larger than in Nd:YAG, determining a low cw threshold.

Nd^{3+} ions in YVO_4 have a large absorption cross section at a wavelength around 809 nm, with a peak value of about 2.7×10^{-19} cm^2 [2.80]. Thus, with a doping level of 1% at. Nd or 1.26×10^{20} Nd ions/cm^3 the absorption coefficient is 34 cm^{-1}. The peak absorption cross section of Nd:YVO_4 for the π direction is about seven times larger than that of Nd:YAG at 808 nm (4.1×10^{-20} cm^2).

The intense pump absorption of 809 nm laser diode radiation allows the use of short cyrstals that absorb most of the incident light. Since the divergence of the pump beam is typically much larger than that of the resonator mode, a crystal capable of absorbing pump radiation in a short length can best match the spot size of the resonator mode. In particular, fiber-coupled diode sources, because of their relatively poor beam quality, have a short Rayleigh range when focused to a small spot size.

Although a high absorption and short active region is desirable from a mode matching point of view, it is in contrast to the requirement of adequate heat dissipation required for high-power operation. A small pump volume increases the thermal gradients and the mechanical stress. It has been shown that the pump power fracture limit of Nd:YVO_4 is inversely proportional to the doping concentration [2.81].For this reason it was found that for higher power operation with pump sources on the order of 30 W the optimum concentration for a Nd:YVO_4 crystal is in the range of 0.25–0.4% Nd [2.82].

Figure 2.13 depicts the $E||c$ polarized spectra of a 10 mm long crystal with a 0.27% doping [2.83]. Peak absorption is centered at 808.7 nm with a line width at room temperature of 2.5 nm FWHM. The broader pedestal absorption arises from other weak Nd lines.

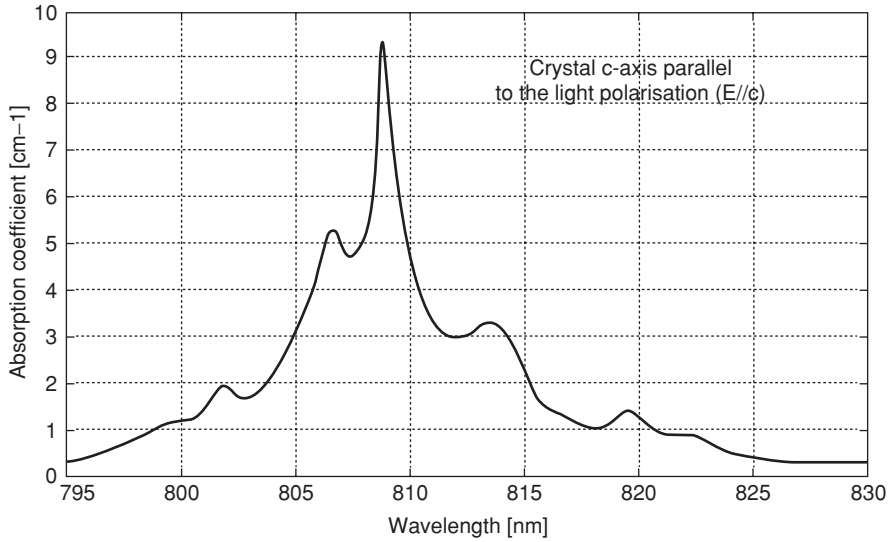


Fig. 2.13. Absorption spectrum of a 0.27% doped Nd:YVO_4 crystal in the region of the 808 nm pump band (after [2.83].)

In an attempt to reduce thermal heating in Nd:YVO_4 a number of systems [2.84, 85] have been pumped at 880 nm directly into the upper laser level as illustrated in Fig. 2.14. The laser emission in Nd:YVO_4 at 1064 nm is the transition $^4F_{3/2}(R_1) \rightarrow {}^4I_{11/2}(Y_1)$. The Nd:$YVO_4$ crystals are traditionally pumped into the strongly absorbing

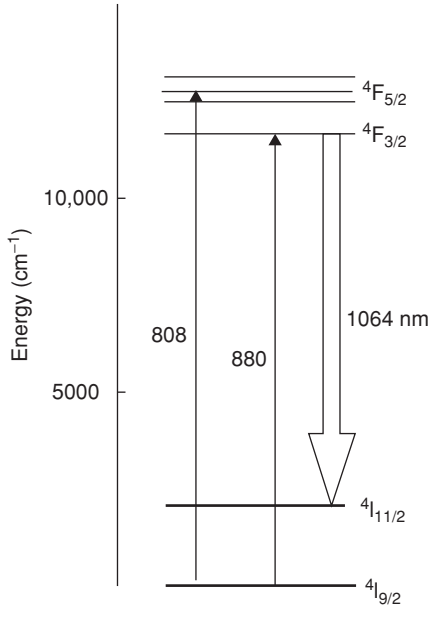


Fig. 2.14. Pumping of Nd:YVO_4 at 808 or 879 nm.

$^4F_{5/2}$ level at 809 nm. An alternative pump transition for Nd:YVO_4 is $^4I_{9/2}(Z_1) \rightarrow {}^4F_{3/2}(R_1)$ at 880 nm. Pumping directly into the upper laser level leads to a reduction of quantum defect heating on account of the smaller difference of the wavelength of the pump and laser radiation. Pumping at the longer wavelength increases the quantum defect efficiency (Stokes factor η_s)from 0.76 to 0.83. An optical-to-optical slope efficiency of 75% with diode laser pumping at 880 nm was reported for a 1 mm thick Nd:YVO_4 crystal doped at 1% [2.84].

The properties of Nd:YVO_4 can best be exploited in an end-pumped configuration and a number of commercial lasser systems are based on fiber-coupled diode arrays pumping a small vanadate crystal. Actually, Nd:YVO_4 is the material of choice for cw endpumped lasers with output power up to about 30 W[2.86–90]. These systems are often also internally frequency doubled to provide output at 532 nm. In endpumped systems the pump beam is usually highly focused and it is difficult to maintain a small beam waist over a distance of more than a few millimeters. In this case a material such as Nd:YVO_4, which has a high absorption coefficient combined with high gain, is very advantageous.

Impressive overall efficiencies have been achieved in Nd:YVO_4 as illustrated in the examples presented in Sects. 3.6.3 and 6.2.3. For cw-pumped, repetitively Q-switched operation, the relatively short upper-state lifetime of Nd:YVO_4 requires high pulse rates of 50–100 kHz in order to achieve average power close to cw performance. The high gain in combination with a short fluorescence lifetime produces relatively short Q-switch pulses compared to Nd:YAG and Nd:YLF. Pulsewidth in repetitively Q-switched systems is typically around 10 ns.

Like most other Nd-doped crystals, Nd:YVO_4 can also be used to generate 1.34 μm radiation. At this wavelength, the slope efficiency is reduced compared to 1.06 μm operation and thermal loading is higher due to the larger quantum defect. An end-pumped Nd:YVO_4 laser with a slope efficiency of 40% and producing 7.3 W of output power in a twice diffraction-limited beam has been reported in [2.83].

2.4 Er:Lasers

Erbium–laser performance is not very impressive in terms of efficiency or energy output. However, erbium has attracted attention because of two particular wavelengths of interest. A crystal, such as YAG, highly doped with erbium produces an output around 2.9 μm, and Er-doped phosphate glass generates an output at 1.54 μm. Both of these wavelenghts are absorbed by water, which leads to interesting medical applications in the case of the 2.9 μm lasers, and to eye safe military rangefinders in the case of the shorter wavelength.

2.4.1 Er:YAG

In 1975 Soviet researchers [2.91] discovered laser operation at room temperature in highly doped Er:YAG, i.e., erbium concentrations at around 50%. Laser emission

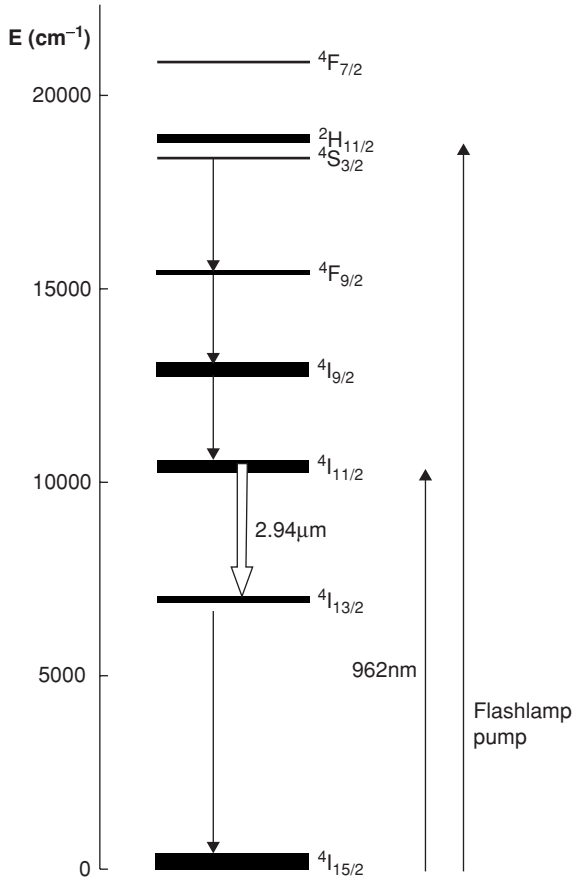


Fig. 2.15. Energy level diagram of Er:YAG for laser action at 2940 nm

occurs at 2940 nm. The laser is of particular interest because its wavelength coincides with a water absorption line. Optical absorption by the water in tissue is extremely large (>3000 cm^{-1}), making potential medical applications such as plastic surgery very attractive.

Figure 2.15 depicts a simplified energy level diagram of Er:YAG. The 2940 nm lasing transition is between the $^4I_{11/2}$ and $^4I_{13/2}$ states of the Er^{3+}ion . The system is a four-level laser because the lower laser level is separated from the ground state $^4I_{15/2}$ by almost 7000 cm^{-1}. The stimulated emission cross section for this laser transition is $\sigma = 3 \times 10^{-20}$ cm^2. Despite a much shorter lifetime of the emitting level ($^4I_{11/2}$) as compared to the terminal level ($^4I_{13/2}$), efficient 2.9 μm room temperature laser emission between these two levels is possible because of very complex energy transfer processes. As a result of up-conversion, and cross relaxation between neighboring Er^{3+}ions in the $^4I_{13/2}$ level, much of the lower laser level population is recycled into the upper laser level, thus overcoming the unfavorable lifetime of the two levels [2.92, 93]. Relatively long pump pulses are required because the up-conversion process in

Er:YAG takes about 100 μs for pumping at 962 nm to bring the system to the cw regime. For this reason there is a minimum pump duration below which the system efficiency decreases.

The most efficient pump process is direct excitation of the upper laser level $^4I_{11/2}$ by laser diodes emitting at a wavelength of 962 nm. Measured absorption coefficient of Er:YAG for the diode emission at this wavelength is 14 cm^{-1}. Excitation with flashlamp pumping is mainly at shorter wavelengths into the $^4F_{7/2}$, $^2H_{11/2}$, and $^4S_{3/2}$ levels as shown in Fig. 2.15. Major absorption occurs for these levels between 480 to 530 nm. The excitation from these higher energy levels of Er^{3+} cascades downward to the upper laser level.

Flashlamp-pumped Er:YAG lasers have a very low system efficiency. A contributing factor is the large quantum defect since the upper laser leval of the 2940 nm transition is pumped mainly by light at a wavelength less than 600 nm. A typical example is a 75 mm long by 6.25 mm diameter 50% doped Er:YAG rod pumped by two flashlamps of 7 mm bore diameter in a double elliptical, silver-coated pump cavity [2.94]. At a pulse duration of 170 μs, the laser produced an output of 600 mJ at an input energy. of 360 J per pulse. The repetition rate was 1 Hz. At higher repetition rates thermal lensing caused a reduction in efficiency and distorted the beam shape.

The system efficiency increases from a fraction of 1% to about 4–5% for laser diode pumped Er:YAG lasers. As an example, Fig. 2.16 depicts the output versus input characteristics of a 1.5-mm-thick Er:YAG hexagonal disk side-pumped with three laser diode bars [2.95]. This particular geometry provides for multiple internal reflection regions of the laser beam. The three quasi cw stacked-array diode lasers emitted at 962 nm with a spectral width of 5 nm (FWHM). The diodes were pulsed at 400 μs at a repetition rate of 100 Hz. The maximum output of 32 mJ of energy was achieved at 230 mJ of pump energy delivered to the crystal. This corresponds to an optical-to-optical efficiency of 14%.

The most efficient Er:YAG lasers are end-pumped monolithic designs. Power outputs around 1 W cw have been achieved [2.96]. Short pulses can be generated by Q-switching Er:YAG lasers with devices such as piezoelectrically controlled frustrated total internal reflection prisms[2.97] or passive devices using bleachable absorption[2.98].

Besides Er:YAG , the crystal Er:YLF is frequently employed for the generation of 2810 nm radiation. A 15% doped Er:YLF crystal, side-pumped by two 40 W diode bars emitting at 980 nm, generated up to 4 W cw output[2.99]. Using an intra-cavity quartz birefringent plate for wavelength selection, tunable output between 2700 and 2800 nm was obtained at specific lines corresponding to particular transitions between $^4I_{11/2}$ and $^4I_{13/2}$ manifolds.

2.4.2 Er:Glass

Erbium has been made to lase at 1.54 μm in both silicate and phosphate glasses. Because of the three-level behavior of erbium and the weak absorption of pump radiation codoping with other rare earth ions is necessary to obtain satisfactory system efficiency. In fact, erbium must be sensitized with ytterbium if the material is to lase

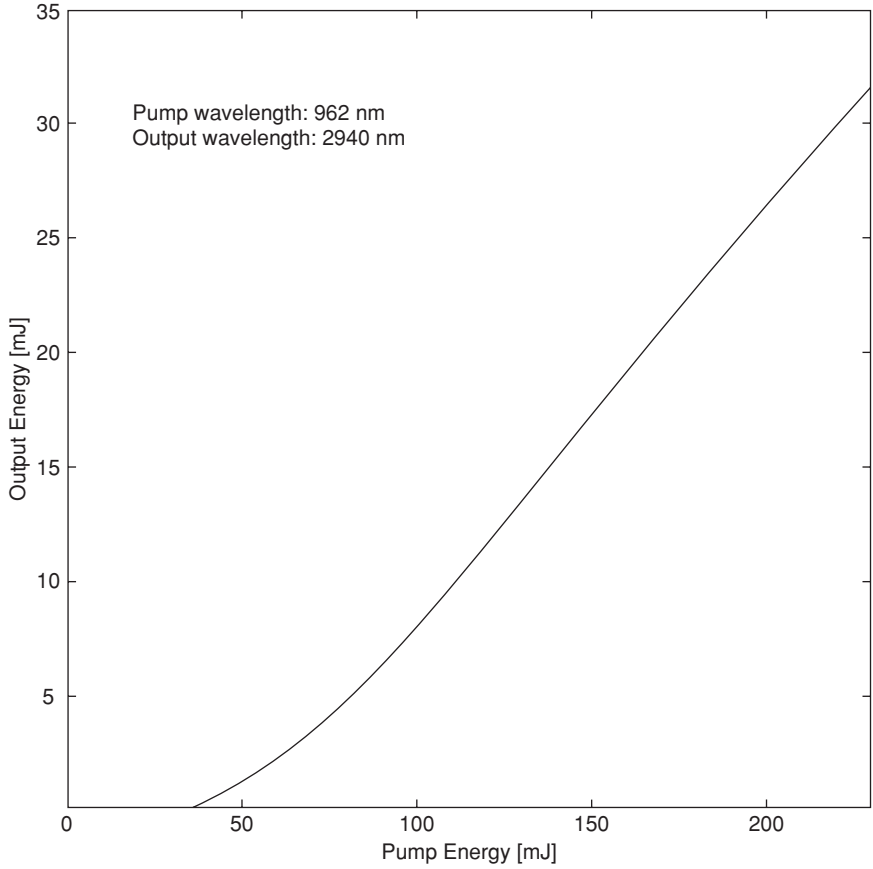


Fig. 2.16. Output vs. input curve for a diode pumped Er:YAG laser at 100 pps (after Ref.2.95)

at all at room temperature. Pump radiation is absorbed by ytterbium, which has an absorption band between 0.9 and 1 μm, and transferred to the erbium ions. The transfer is illustrated in Fig. 2.17. In the codoped Er:Yb:glass, radiation from a flashlamp or laser diode pumps the strong $^2F_{7/2}$–$^2F_{5/2}$ transition in Yb^{3+}. Because of the good overlap between the upper states of Yb^{3+} and Er^{3+}, the excited Yb^{3+}ions transfer energy to the $^4I_{11/2}$ level of Er^{3+}. The erbium ions then relax to the upper laser level $^4I_{13/2}$ and lasing occurs down to the $^4I_{15/2}$ manifold.

Laser action terminates at a Stark level within the ground maniflod. At room temperature all levels of the terminal $^4I_{15/2}$ manifold are populated to some degree, thus this transition forms a three-level laser scheme with a correspondingly high threshold.

For flashlamp pumping, the efficiency of Er:glass can be further improved by adding Cr^{3+} in addition to Yb^{3+}. The Cr^{3+}ions absorb flashlamp radiation in two broadbands centered at 450 and 640 nm, and emit radiation in a broadband centered

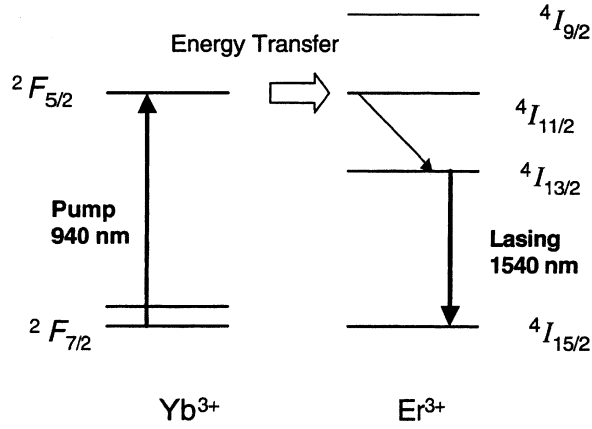


Fig. 2.17. Energy level diagram in codoped Er, Yb:glass

at 760 nm. This allows energy to be transferred from Cr^{3+} to the $^4I_{9/2}$ and $^4I_{11/2}$ states of Er^{3+} and the $^2F_{5/2}$ state of Yb^{3+} .

With the development of strained layer InGaAs laser diodes, which have emission between 0.9 and 1 μm, it is now possible to pump the strong Yb^{3+} transition $^2F_{7/2} - {}^2F_{5/2}$. Diode pumping at 940 nm has dramatically improved the efficiency and average power achievable from Er:glass lasers.

The absorption of pump radiation by Yb^{3+} and efficient transfer to Er^{3+} is possible because the transfer rate from Yb to the Er transition is 10 times greater than the $^2F_{5/2}$ relaxation rate of Yb^{3+}. In particular the $^4I_{11/2}$ relaxation rate of Er is less than 10 μs, which allows rapid population of the Er^{3+} lasing state, while minimizing energy back transfer to Yb^{3+}.

The time required for transfer of energy from Yb^{3+} to Er^{3+}, and then for the $Er^{3+4}I_{11/2}$ manifold to relax to the $^4I_{13/2}$ state causes a time delay between the pump pulse and output laser pulse that is typical of Er:Yb:glass and depends on the pump level.

Because of the inhomogeneous broadening of the transition in glass, the absorption spectrum of Er:Yb:phosphate glass is smooth and continuous, allowing pumping at virtually any wavelength from 920 to 1000 nm as illustrated in Fig. 2.18. Material properties of Er:Yb:glass are listed in Table 2.8. The long fluorescence lifetime of Er^{3+} and the broad spectral absorption of Yb^{3+} are fortuitous for laser diode pumping.

The laser diode pumps of Er:glass lasers designed for military applications are typically operated at around 940 nm, rather than at the peak absorption wavelength shown in Fig.2.18. At this wavelength, there is a broad absorption band where the absorption coefficient is between 4 and 6 cm^{-1}. Pumping in this spectral region allows operation of the pump laser diodes over a large temperature range without active temperature control. When compared with flashlamp pumping, the diode pump is over an order of magnitude more efficient and produces less heat.

Figure 2.19 illustrates the performance of a diode pumped Er:Yb: phosphate glass laser [2.100]. The 2 mm diameter and 10 mm long laser rod was side-pumped by two

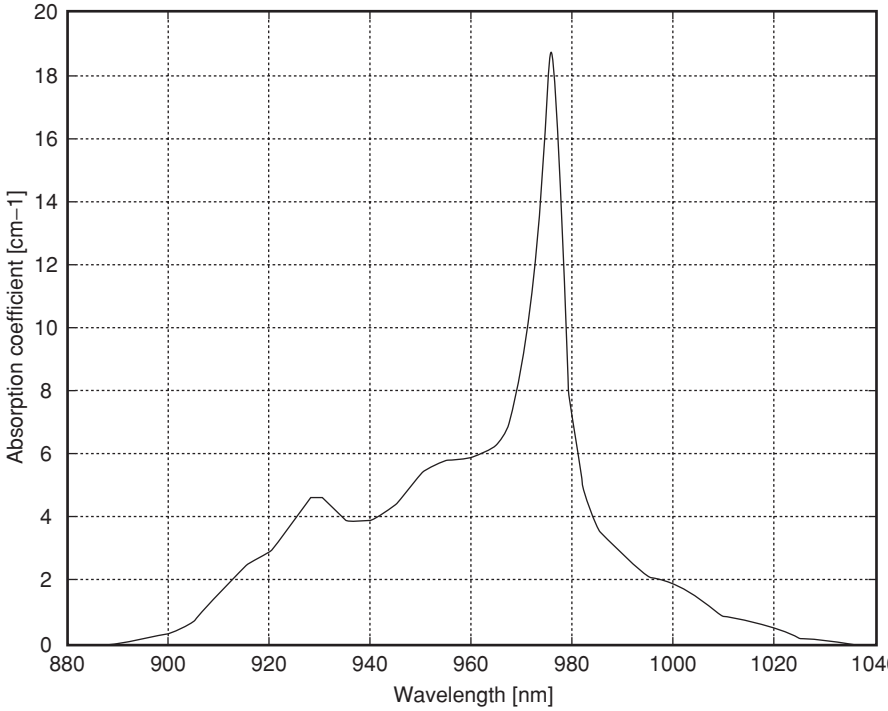


Fig. 2.18. Absorption spectrum of Er:Yb:phosphate glass [2.100]

diode arrays. Each array consisted of a stack of three 1-cm bars which had a 7-mm FWHM bandwidth peaked at 973 nm. The pulse width was limited by the power supply to 1 ms. At the maximum output of 20.5 mJ, the optical-to-optical efficiency was 8.6% and the system achieved a wall plug efficiency of 2.7%.

Small hand-held rangefinders are the major application of Er:glass lasers. For these applications the lasers have to be Q-switched. This is accomplished typically with spinning prisms, frustrated total internal reflection (FRIR)devices or intra-cavity bleachable absorbers.

A Q-switched Er:glass laser operating up to 50 Hz and producing 14 mJ Q-switched pulses at 25 Hz has been reported in [2.101]. The pump pulse width was

Table 2.8. Material properties of an erbium doped phosphate glass

Emission wavelength	1.54 μm
Fluorescent lifetime	8 ms
Index of refraction at 1.54 μm	1.531
dn/dT	$63 \times 10^{-7}/^{\circ}\mathrm{C}$
Thermal expansion (α)	$124 \times 10^{-7}/^{\circ}\mathrm{C}$
Thermo-optic coefficient (W)	$-3 \times 10^{-7}/^{\circ}\mathrm{C}$

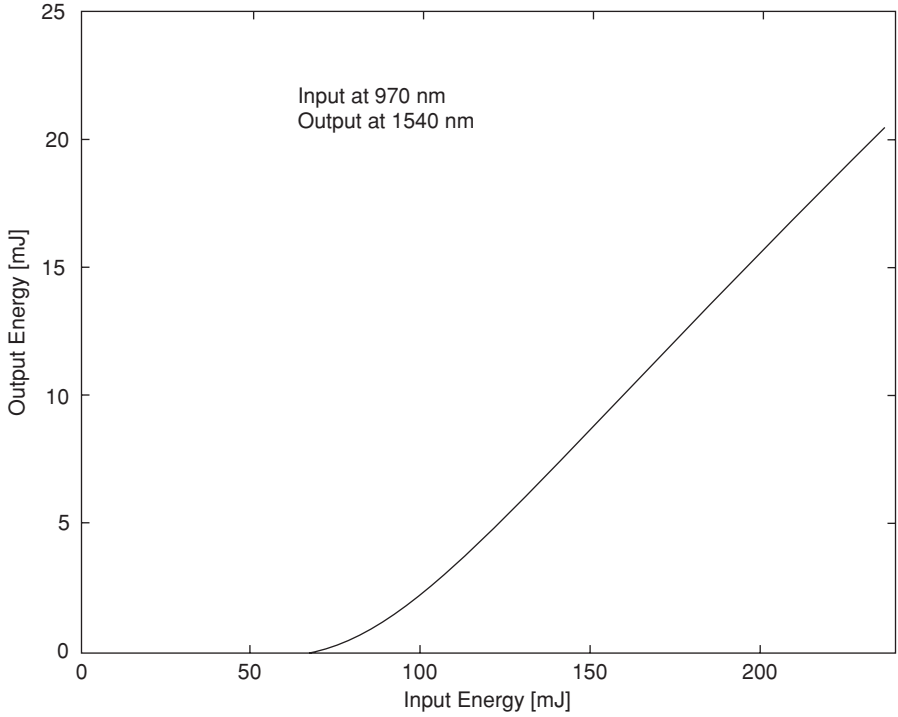


Fig. 2.19. Output vs. input of a diode pumped Er:Yb:phosphate glass laser [2.100]

5 ms with the diode arrays centered at 940 nm. The 2.5 mm diameter and 33 mm long Er:Yb:glass rod was side-pumped by 18 one centimeter bars. Total pump energy was 1.3 J. The Q-switch was a FTIR device. Since FTIR Q-switches are not polarization sensitive, thermal distortions that could lead to large depopulation losses in electro-optical Q-switches are not a problem.

A passively Q-switched microlaser producing 50 kw of peak power at 20 Hz has been described in [2.102]. The Co^{2+}:$MgAl_2O_4$ (Co:Spinel) saturable absorber Q-switch produced 2 ns pulses. In this design a single-stripe laser diode with 4 W output end-pumped a $2 \times 2 \times 3$ mm Er:doped phosphate glass "mini brick." The complete laser can be packaged on a TO-3 header and the pulse energy of 100 μJ is sufficient for range applications up to 2 km.

2.5 Tunable Lasers

In a typical laser, such as Nd:YAG, the laser transition occurs between discrete energy states which produces a narrow line width output beam. Tunability of the emission in solid-state lasers is achieved when the stimulated emission of photons is intimately coupled to the emission of vibrational quanta (phonons) in a crystal lattice.

This electron–phonon coupling creates vibrational sublevels that spread the energy levels into bands, in this way laser transition can take place over a range of energies. In these "vibronic" lasers, the total energy of the lasing transition is fixed, but can be partitioned between photons and phonons in a continuous fashion. When a laser transition occurs between these coupled vibrational and electronic states, vibrational energy, i.e. a phonon, is either emitted or absorbed with each electronic transition.

Vibronic lasers have gain over a broad range of wavelengths which means they can produce either tunable output or ultra-short pulses (see Chap. 9). The large gain bandwidth of tunable lasers leads to some trade-off with other important material parameters. From (1.41) it follows that the excited state lifetime $\tau_f = 1/A_{21}$ and the cross section σ for stimulated emission is proportional to the inverse of the gain bandwidth $\Delta\nu$. By virtue of having a large bandwidth, tunable laser crystals have either a small stimulated emission cross section or a short fluorescence lifetime. Both parameters determine the operating characteristics of these lasers.

A small product ($\sigma\tau_f$) leads to a high threshold for cw operation (see Chap. 3), a short fluorescence time τ_f makes pumping with flashlamps or laser diodes problematic or impossible, and a small σ requires a very intense pump source to reach threshold.

Typically, vibronic lasers are four-level systems and the laser transition occurs from the upper level to a vibrationally excited sublevel of the ground state. The ions in the lower laser level drop back to the ground level by releasing vibrational energy. The actual gain curve depends on temperature because the vibrational sublevels of the ground manifold—the lower laser level—are thermally populated. Higher temperatures populate higher vibrational levels, preventing the laser from oscillating at the shorter wavelength.

The history of tunable solid-state lasers can be traced back to work performed over 40 years ago at Bell Laboratories. In 1963, Bell-Labs researchers reported the first vibronic laser, a nickel-doped magnesium fluoride (Ni:MgF_2) device [2.103]. The same group later built a series of vibronic lasers using nickel, cobalt, or vanadium as the dopant and MnF_2, MgO, MgF_2, ZnF_2, or $KMgF_3$ as the host crystal [2.104]. Tunable in the 1.12–2.17 μm range, these flashlamp-pumped lasers had a serious drawback: they operated only when cooled to cryogenic temperatures. Despite these early results, this field lay dormant for more than a decade, probably because of the need for cryogenic cooling of the laser material, the emergence of Nd:YAG, and the concentration on dye lasers and color-center lasers. The first room-temperature vibronic laser, reported by Bell Labs in 1974, was a flashlamp-pumped Ho:BaY_2F_8 device emitting at 2.17 μm [2.105].

In 1977, the crystal alexandrite (chromium-doped $BeAl_2O_4$) was made to lase on a vibronic transition [2.106, 107]. The crystal field strength at the chromium site in alexandrite is sufficiently low to permit thermal activation of broad $^4T_2$ fluorescence. The result is a low-gain, four-level laser tunable in the range of 0.7–0.8 μm.

During the mid-1970s, research started on a variety of divalent transition-metal doped crystals such as Ni^{2+}, V^{2+}, and Co^{2+} at MIT Lincoln Laboratory [2.108]. Most of the materials investigated, such as V:MgF_2, suffered from excited state absorption, which reduces the net gain to an unacceptably low level. A notable exception is Co^{2+}:MgF_2, which turned out to be a useful laser.

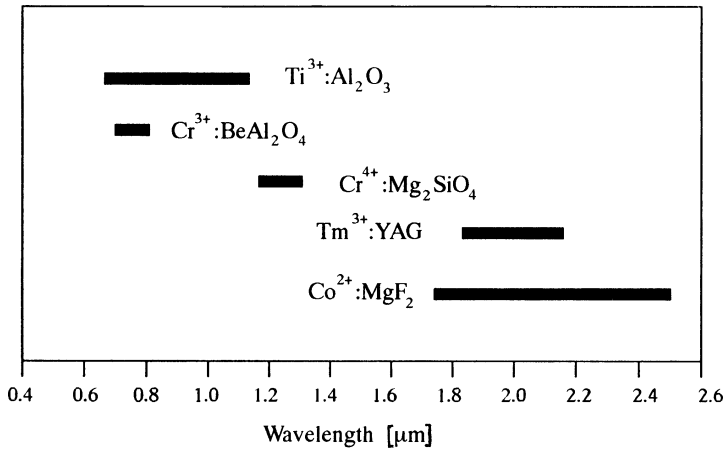


Fig. 2.20. Spectral range of several tunable lasers

If pumped by a 1.3 μm Nd laser, the cobalt laser is tunable from 1750 to 2500 nm. This earlier work resulted also in the discovery of the Ti:sapphire laser by Moulton in 1982 [2.109]. In the sapphire host, Ti^{2+} exhibits no appreciable excited-state absorption and therefore has a tuning range that spans virtually its entire fluorescence emission wavelength range.

The spectral ranges of typical tunable lasers are shown in Fig. 2.20.

Chromium Lasers

Chromium has enjoyed considerable success as a tunable-laser ion due to the special nature of its trivalent d^3 electronic configuration. Particular attributes of Cr over other transition metals are its chemical stability, broad pump bands, large energy-level splitting, and reduced excited state absorption (ESA). These advantages have led to at least a dozen crystals being demonstrated as good laser hosts for Cr. Chromium has a laser tuning range of about 100 nm, with the center wavelength shifted by the particular crystal host.

Alexandrite. Cr in chrysoberyl ($BeAl_2O_4$) lases in the 700–800 nm range and was the first tunable ion solid-state laser considered for practical use. Details of this commercially available laser material are given in Sect. 2.5.1.

Cr:GdScGa-Garnet. Cr^{3+}-doped Ga garnets present a class of transition-metal ion lasers which can operate pulsed as well as cw at room temperature [2.110–113]. Because of a low-crystal field at the Cr site, the $^4A_2 - {}^4T_2$ splitting is nearly equal to the $^4A_2 - {}^4T_2$ separation. Thus, in contrast to ruby or alexandrite, the fluorescence is totally dominated by the broadband four-level $^4T_2 \rightarrow {}^4A_2$ transition.

Garnet crystals are described by the formula $C_3A_2D_3O_{12}$, where one chooses large ions A = Ga, Sc, Lu for the octahedral site, D = Ga for the tetrahedral site, and C = Y,

Gd, La, Lu for the dodecahedral site. Broadband four-level fluorescence has been obtained in the 700–950 nm spectral range from Cr-doped YGG, YScGG (YSGG), GGG, GdScGG(GSGG), and LaLuGG(LLGG) with lifetimes ranging from 240 to 70 μs, respectively. The crystals are grown by the standard Czochralski technique at $\approx 1750^{\circ}$C.

One compound, Cr^{3+}-doped GdScGa-garnet, has received particular attention. In Cr^{3+} -doped GdScGa-garnet, the *R*-line fluorescence is totally absent and because of a large 2400 cm^{-1} Stokes shift of the $^4T_2$ Level, the whole fluorescence is channelled into the broadband (four level) $^4T_2 \rightarrow {}^4A_2$ transition. Pulsed and cw laser action has been obtained from Cr:GSGG over a tuning range from approximately 700 to 900 nm. The development of the alexandrite and Ti:sapphire lasers, which overlap the tuning range of Cr:GSGG have overshadowed this material, since the former can be flashlamp pumped and the latter has a wider tuning range.

Cr:$KZnF_3$. This fluorine perovskite was the second tunable solid-state laser material (after alexandrite) to be offered commercially [2.114]. Cr:$KZnF_3$ operates from 785 to 865 nm, with good slope efficiency when laser pumped between 650 and 700 nm. Like Cr:GSGG, this material has been displaced by the more versatile Ti:sapphire laser.

Cr:Forsterite. Both pulsed and cw laser operation has been achieved in Cr^{4+}:Mg_2SiO_4 with Nd:YAG lasers at 1.06 μm or 532 nm as pump sources [2.115–117]. This laser is of interest because the tuning range covers the spectral region from 1167 to 1345 nm, which is not accessible with other lasers. A distinguishing feature of laser actions in Cr:Mg_2SiO_4 is that the lasing ion is not trivalent chromium (Cr^{3+}) as is the case with other chromium-based lasers but the active ion in this crystal is tetravalent chromium (Cr^{4+}) which substitutes for silicon (Si^{4+}) in a tetrahedral site. Single crystals of Cr-doped forsterite are grown by the Czochralski method. Forsterite has a fluorescence lifetime of 25 μs and therefore has to be pumped by another laser. Stimulated emission cross section is 1.44×10^{-19} cm^2, about one-fourth of Nd:YAG.

One of the pump bands of forsterite spans the region ranging 850–1200 nm. Therefore, pulsed or cw Nd:YAG lasers are employed to pump fosterite lasers. Generation for short mode-locked pulses is the main attraction of this material (see Chap. 9).

Cr:LiSAF. Cr^{3+}-doped $LiSrAlF_6$ has a tuning range from 780 to 920 nm and can be flashlamp and diode pumped. Very large crystals of high optical quality can be grown from this material. Cr:LiSAF lasers are particularly important for femtosecond pulse generation and will be discussed in Sect. 2.5.3 and Chap. 9.

Co:MgF_2

Interest in mid-IR lasers is stimulated by remote sensing and medical applications. Room temperature operation of Co-, Tm-, Ho-, and Er-doped materials has made this spectral region accessible to practical applications.

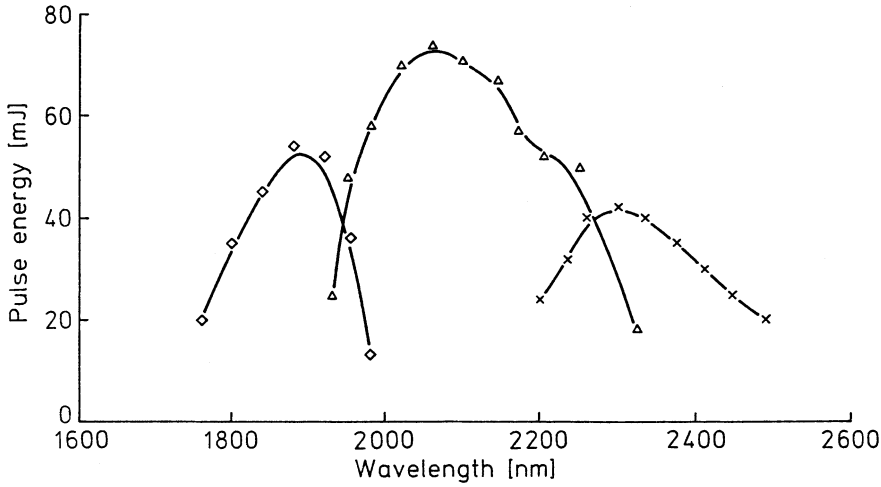


Fig. 2.21. Tuning range of the Co:MgF_2 laser [2.118]

Cobalt-doped magnesium fluoride (Co^{2+}:MgF_2) has a particularly wide tuning range that extends from 1750 to 2500 nm. With flashlamp pumping, the laser requires cryogenic cooling. For this reason not much attention was given to this material. After it was discovered that room temperature operation is possible if the Co:MgF_2 crystal is pumped by a 1.32 μm Nd:YAG or Nd:YLF laser, commercial versions became available. Figure 2.21 shows the tuning range of the Co:MgF_2 laser, which requires different sets of optics to span the whole range.

Pulsed room temperature versions emit average powers on the order of a fraction of 1W. Powerful Co:MgF_2 lasers have achieved outputs up to 980 mJ at 10 Hz repetition rate [2.118]. Laser action is between the $^4T_2$ and $^4T_1$ state of Co^{2+}. The role of the Co:MgF_2 as a tunable source for IR wavelengths has been diminished lately because Nd:YAG lasers, wavelength shifted with an OPO, can cover the same spectral region.

Titanium Laser

The Ti:sapphire laser has an exceptionally wide tuning range and a large gain cross section. Also, large, high-quality crystals are commercially available. These attributes have led to the use of this material for many laser applications. Further details will be discussed in Sect. 2.5.2.

Rare-Earth Tunable Lasers

Tm- and Ho-doped YAG, YLF, and YAP lasers are primarily employed as laser sources in the 2 μm region, a wavelength of interest for certain medical applications and coherent radar systems. However, limited tunability can also be achieved with these lasers. In the previous examples, tunability was afforded by the 3d electron of the transition-metal ions Cr^{3+} and Ti^{3+}. In Tm^{3+}:YAG, for example, the considerable

phonon broadening and high multiplicity of the Stark levels of the 4f electron provides tunability from 1.87 to 2.16 μm (Sect. 2.5.4). Similarly, holmium lasers have some tunability around 2.067 μm. For example, a diode-pumped Ho:Tm:YLF laser was tuned with an etalon between 2.06 and 2.07 μm [2.119]. Holmium lasers are usually codoped with Tm to provide increased absorption for the pump source. Although not particularly considered a tunable laser, Yb:YAG has tunability from 1.018 to 1.053 μm [2.120]. This laser is mainly of interest for high-power generation.

Tm, Ho, and Yb lasers have been known for years, but flashlamp pumping is not particularly efficient in these three-level lasers. The fact that these crystals can be pumped with laser diodes has generated renewed interest in these lasers materials. Tm:YAG is discussed in Sect. 2.5.4 and Yb:YAG in Sect. 2.6.

2.5.1 Alexandrite Laser

Alexandrite ($BeAl_2O_4$:Cr^{3+}) developed by Walling et al. [2.121] is the common name for chromium-doped chrysoberyl—one of the olivine family of crystals—with four units of $BeAl_2O_4$ forming an orthorhombic structure. The crystal is grown in large boules by the Czochralski method much like ruby and YAG. Laser rods up to 1 cm in diameter and 10 cm long with a nominal 2-fringe total optical distortion are commercially available. The chromium concentration of alexandrite is expressed in terms of the percentage of aluminum ions in the crystal which have been replaced by chromium ions. The Cr^{3+} dopant concentration, occupying the Al^{3+} sites, can be as high as 0.4 at.% and still yield crystals of good optical quality. A concentration of 0.1 at.% represents 3.51×10^{19} chromium ions per cubic centimeter.

Alexandrite is optically and mechanically similar to ruby, and possesses many of the physical and chemical properties of a good laser host. Hardness, strength, chemical stability, and high thermal conductivity (two-thirds that of ruby and twice that of YAG) enables alexandrite rods to be pumped at high average powers without thermal fracture. Alexandrite has a thermal fracture limit which is 60% that of ruby and five times higher than YAG. Table 2.9 lists the chrysoberyl material properties [2.122].

Table 2.9. Material parameters of alexandrite

Laser wavelength (nm)	700–818
Stimulated emission cross section (cm^2)	1.0×10^{-20}
Spontaneous lifetime (μs)	260 ($T = 298$ K)
Doping density (at.%)	0.05–0.3
Fluorescent linewidth (nm)	100
Gain coefficient for 1 J/cm^3 stored energy (cm^{-1})	0.038–0.19
Index of refraction (750 nm)	$E \| \| b$ 1.7421
Thermal expansion	$\| \| b\, 6.1 \times 10^{-6}$ /K
Thermal conductivity (W/cm K):	0.23
Melting point (°C)	1870
Hardness (kg/mm^2)	2000

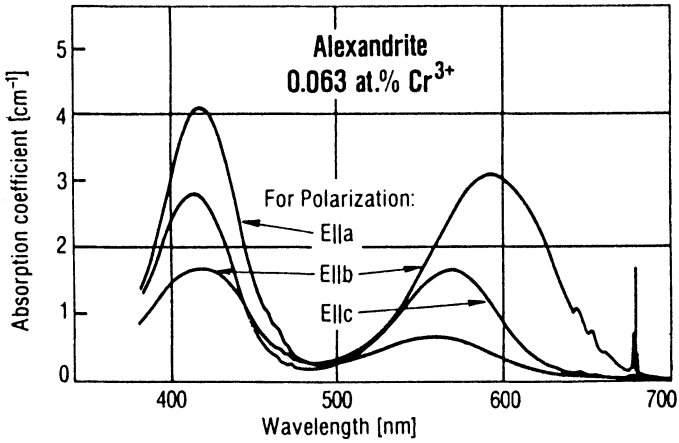


Fig. 2.22. Absorption spectrum of alexandrite [Allied Corps. Data Sheet]

Because of its orthorhombic structure, alexandrite is biaxial with the principal axes of the index ellipsoid along the crystallographic axes. Light emitted from the laser is polarized with the E vector parallel to the b axis. The gain in the $E \parallel b$ polarization is 10 times that in the alternate polarizations. Alexandrite lases at room temperature with flashlamp pumping throughout the range 701–818 nm. The alexandrite absorption bands are very similar to those of ruby, and span the region from about 380 to 630 nm, with peaks occurring at 410 and 590 nm.

The absorption spectrum of alexandrite shown in Fig. 2.22 is compatible with pumping by flashlamps. Alexandrite lasers can also operate cw when pumped by arc lamps. But most commercial alexandrite lasers are pumped by flashlamps. The absorption peak near 680 nm shown in Fig. 2.22 has been exploited to pump alexandrite with diode lasers [2.123].

The laser gain cross section increases from 7×10^{-21} cm^2 at 300 K to 2×10^{-20} cm^2 at 475 K, which results in improved laser performance at elevated temperature. The 260 μs, room-temperature fluorescence lifetime permits effective energy storage and Q-switched operation.

Alexandrite can operate both as a four-level vibronic laser and as a three-level system analogous to ruby. As a three-level laser, it has a high threshold, fixed output wavelength (680.4 nm at room temperature), and relatively low efficiency. Obviously, the primary interest of alexandrite lies in its vibronic nature.

The basic physics of the four-level alexandrite laser can be discussed with reference to the energy level diagram (Fig. 2.23). The $^4A_2$ level is the ground state, and $^4T_2$ is the absorption state continuum. Vibronic lasing is due to emission from the $^4T_2$ state to excited vibronic states within $^4A_2$. Subsequent phonon emission returns the system to equilibrium. Since alexandrite is an intermediate crystal field material ($E \approx 800$ cm^{-1}) there is coupling between the ^2E state and the $^4T_2$. The lifetimes of each of these states is 1.5 ms and 6.6 μs, respectively. The two R lines emitted from ^2E occur in the vicinity of 680 nm, as for ruby. The terminal laser level is a

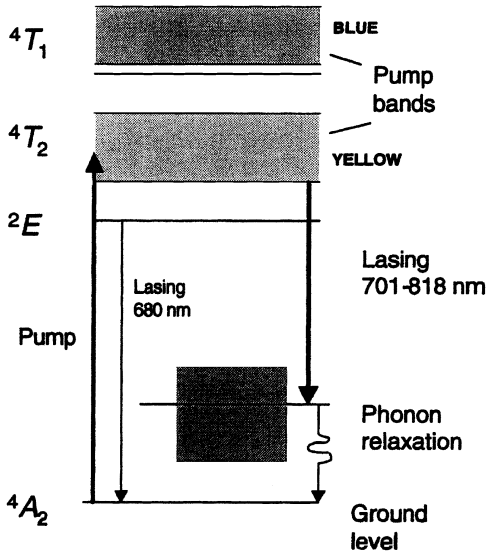


Fig. 2.23. Simplified energy level diagram for chromium ions in alexandrite

set of vibrational states well above the ground state. The initial laser level is a level 800 cm^{-1} above a long-lived storage level and in thermal equilibrium with it.

Because of the vibronic nature of the alexandrite laser, the emission of a photon is accompanied by the emission of phonons. These phonons contribute to thermalization of the ground-state vibrational levels. The laser wavelength depends on which vibrationally excited terminal level acts as the transition terminus; any energy not released by the laser photon will then be carried off by a vibrational phonon, leaving the chromium ion at its ground state.

As the temperature increases, the gain of alexandrite increases, the gain peak shifts to a longer wavelength, and the fluorescence lifetime decreases. The four-level model can be used to predict the temperature dependence of the laser performance. The ^2E state acts as a storage level for $^4T_2$. Thus, as the temperature of alexandrite increases, the vibronic continua in $^4T_2$ are successively populated from ^2E in accordance with the Boltzmann distribution and the stimulated emission cross-section increases.

However, raising the temperature also tends to populate the terminal levels, especially those which lie closest to the ground level and which therefore correspond to the highest-energy (shortest-wavelength) photons. Since laser performance is highest with a maximally populated initial level and a minimally populated terminal level, it can be seen that increasing the temperature has two conflicting effects. The result is that performance is positively affected by temperature increases only for wavelengths above 730 nm.

Guch [2.124] evaluated the performance of a flashlamp-pumped alexandrite laser at temperatures from ambient to 310°C. As illustrated in Fig. 2.24a, the variation in laser output over the 34°–310°C range is dramatic. The threshold performance indicates that laser gain rises significantly, as temperature increases. Figure 2.24b illustrates laser output energy as a function of temperature for a fixed input to the

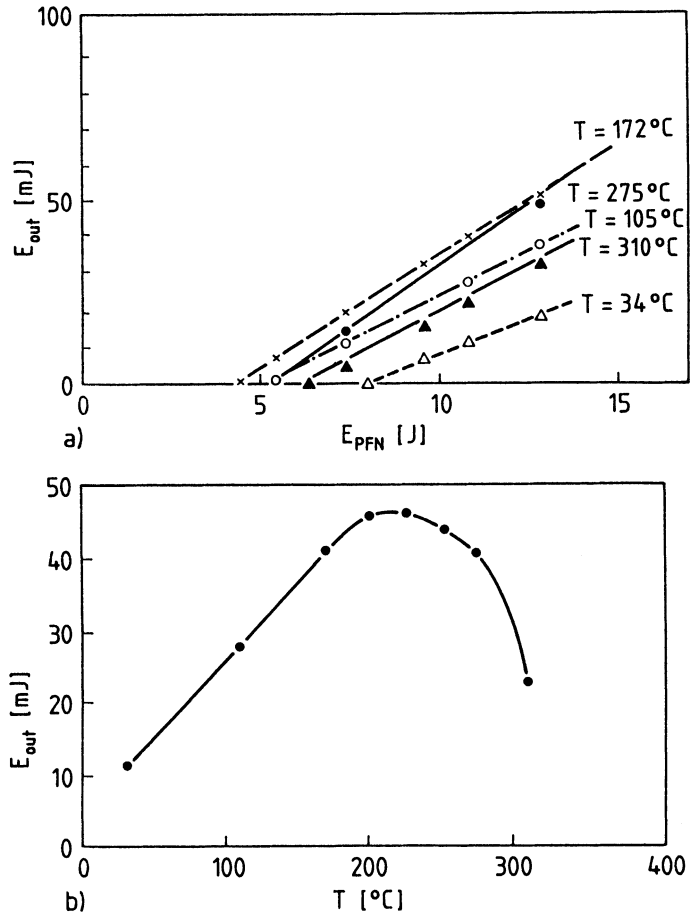


Fig. 2.24. Temperature dependence of alexandrite (a) Alexandrite laser energy as a function of pump energy at temperatures from 34 to 310°C. (b) Alexandrite laser output energy as a function of temperature for fixed 10.8-J flashlamp output [2.124]

flashlamp. The ability of alexandrite lasers to sustain high gain and efficiency at temperatures above those normally encountered in solid-state lasers is particularly striking.

For a fixed lamp pulse there is an optimum temperature at which the output peaks because the gain increases with temperature, but the fluorescent lifetime decreases, At higher temperatures the fluorescence lifetime becomes shorter than the flashlamp pulse duration and stored energy is lost as fluorescence.

The development of the alexandrite laser has reached maturity after over 20 years of efforts. Its high average-power performance is about 100 W if operated at 250 Hz [2.125]. Overall efficiency is close to 0.5%. Tunability over the range of approximately 700–818 nm has been demonstrated with tuning accomplished in a manner similar to dye lasers: a combination of etalons and birefringent filters. With these standard

spectral control devices 0.5 cm^{-1} linewidths and tunability over 150 nm has been achieved. Alexandrite has been lased in pulsed and cw modes; it has been Q-switched and mode locked.

A rod 10 cm long and 0.63 cm in diameter, when lased in a stable resonator, yields over 5 J long-pulsed and as much as 2 J with pulse duration less than 30 ns when Q-switched [2.122]. The reason for such high output energies is the fact that alexandrite is a low-gain medium.

2.5.2 Ti:Sapphire

Since laser action was first reported [2.109], the Ti:Al_2O_3 laser has been the subject of extensive investigations and today it is the most widely used tunable solid-state laser. The great interest in this material arises from the broad vibronic fluorescence band which allows tunable laser output between 670 and 1070 nm. Besides the broad tuning range of about 400 nm, Ti:sapphire possesses a large gain cross section that is comparable to Nd:YAG.

In this material, a Ti^{3+} ion is substituted for an Al^{3+} ion in Al_2O_3. Laser crystals, grown by the Czochralski method, consist of sapphire doped with 0.1% Ti^{3+} by weight. The absorption and fluorescence spectra for Ti:Al_2O_3 are shown in Fig. 2.25.

Crystals of Ti:Al_2O_3 exhibit a broad absorption band, located in the blue-green region of the visible spectrum with a peak around 500 nm. This is a wavelength region readily accessible with argon-ion and frequency-doubled Nd:YAG lasers, Both of these lasers are the most frequently employed pump sources for Ti:sapphire.

A relatively weak absorption band is observed in the IR region, which has been shown to be due Ti^{3+}–Ti^{4+} pairs. The presence of Ti^{4+} ions causes detrimental absorption that interferes with efficient laser operation. Optimized crystal growth techniques and additional annealing processes have drastically reduced this absorption band compared to earlier crystals.

The fluorescence peaks at 780 nm, with a 180 nm bandwidth (FWHM). Therefore, the tunable output from commercial Ti:sapphire lasers is highest between about 700 and 900 nm.

A schematic energy level diagram of Ti:sapphire is shown in Fig. 2.26. The laser transition is between the ^2E excited state and the $^2T_2$ ground state. Optical pumping excites Ti^{3+} to the upper laser level, which then relaxes to the bottom of the vibronic band before making the laser transition. Vibrational relaxation then drops ions to the bottom of the ground-level vibronic band. A strong interaction between the Ti atoms and host crystal, combined with a large difference in electron distribution between the two energy levels, makes the transition linewidth broad.

The energy level structure of the Ti^{3+} ion is unique among transition-metal laser ions in that there are no d-state energy levels above the upper laser level. The simple energy-level structure ($3d^1$ configuration) eliminates the possibility of excited-state absorption of the laser radiation, an effect which has limited the tuning range and reduced the efficiency of other transition-metal-doped lasers.

The laser parameters of Ti:Al_2O_3 are listed in Table 2.10. The outstanding features of Ti:sapphire are the broad fluorescence linewidth and the high stimulated emission cross-section. A drawback is the short fluorescence lifetime.

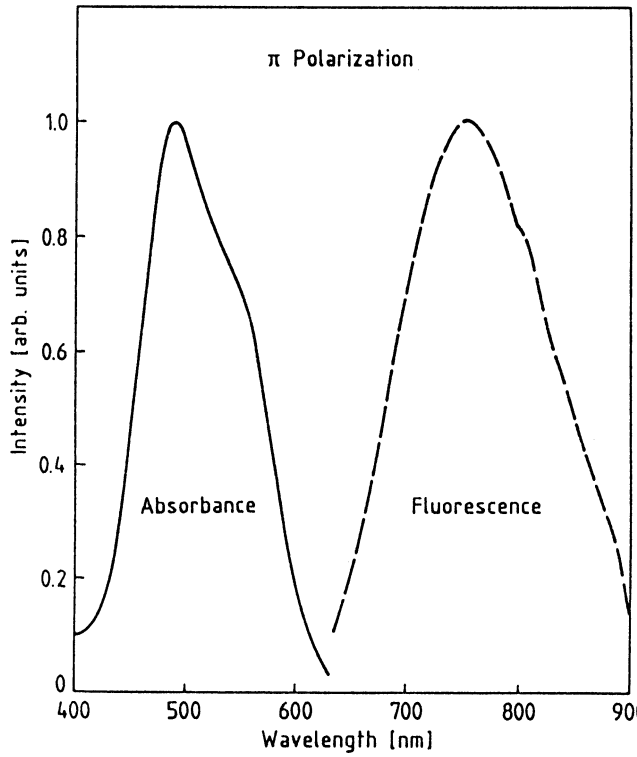


Fig. 2.25. Absorption and fluorescence spectra of the Ti^{3+} ion in Al_2O_3 (sapphire) [2.126]

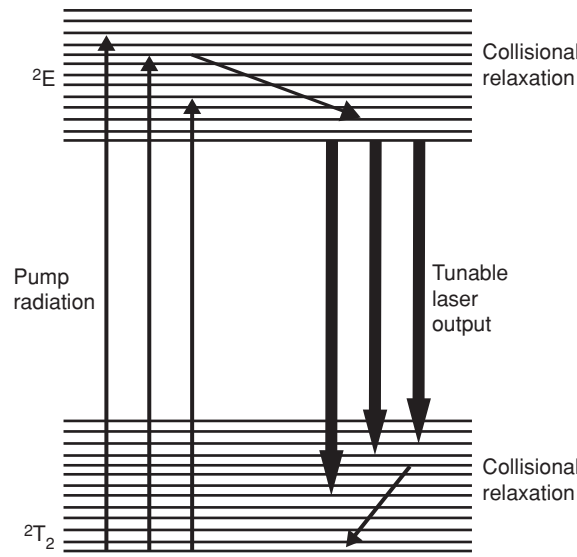


Fig. 2.26. Schematic energy level diagram of Ti:sapphire

Table 2.10. Laser parameters of Ti:Al_2O_3

Index of refraction	1.76
Fluorescent lifetime	3.2 μs
Fluorescent linewidth (FWHM)	230 nm
Peak emission wavelength	780 nm
Peak stimulated emission cross section	
parallel to *c*-axis	$\sigma_{\|\|} \sim 4.1 \times 10^{-19}$ cm^2
perpendicular to *c*-axis	$\sigma_{\perp} \sim 2.0 \times 10^{-19}$ cm^2
Stimulated emission cross section	
at 0.795 μm	$\sigma_{\|\|} = 2.8 \times 10^{-19}$ cm^2
Quantum efficiency of converting a 0.53 μm photon into an inverted site	$n_Q \approx 1$
Saturation fluence at 0.795 μm	$E_s = 0.9$ J/cm^2

Besides having favorable spectroscopic and lasing properties, one other advantage of Ti:Al_2O_3 are the material properties of the sapphire host itself, namely very high thermal conductivity, exceptional chemical inertness, and mechanical rigidity. Titanium sapphire is available from commercial vendors in sizes of 3.5 cm diameter by 15 cm long and, as a result of the well-developed growth technology for sapphire, of good optical quality.

Ti:sapphire lasers have been pumped with a number of sources such as argon and copper vapor lasers, frequency doubled Nd:YAG and Nd:YLF lasers, as well as flashlamps.

Flashlamp pumping is very difficult to achieve in Ti:sapphire because a very high pump flux is required. The reason is the short fluorescence lifetime of 3.2 μs which results in a small product of stimulated emission cross-section times fluorescence lifetime ($\sigma\tau_f$). The population inversion in a laser required to achieve threshold is inversely proportional to $\sigma\tau_f$ as will be shown in Sect. 3.1. However, improvements in crystal quality, which lead to the removal of residual absorption bands, in combination with special flashlamps have resulted in output energies of 3 J per pulse at 2% efficiency. The flashlamps designed for high wall loadings were spectrally enhanced by using a dye surrounding the laser rod to convert near-UV light from the flashlamp into blue-green fluorescence which is within the absorption band of Ti:sapphire [2.127]. With design improvements in the lamp-discharge circuit and the pump cavity, an average power of 220 W at an efficiency of 2.2% has been achieved [2.128].

Commercial Ti:sapphire lasers are pumped by argon lasers to obtain cw output, and by frequency-doubled Nd:YAG or Nd:YLF lasers for pulsed operation. In the cw mode, typical performance is close to 1 W output with a 5 W argon pump.

Figure 2.27 depicts typical output characteristics of argon-ion pumped Ti:sapphire lasers. Without wavelength selection, the spectral output is near the peak of the gain curve. Wavelength selection and tuning is typically achieved by angular adjustment of a birefringent filter. In order to cover the entire wavelength range of Ti:sapphire, a change of the resonator mirrors is also required.

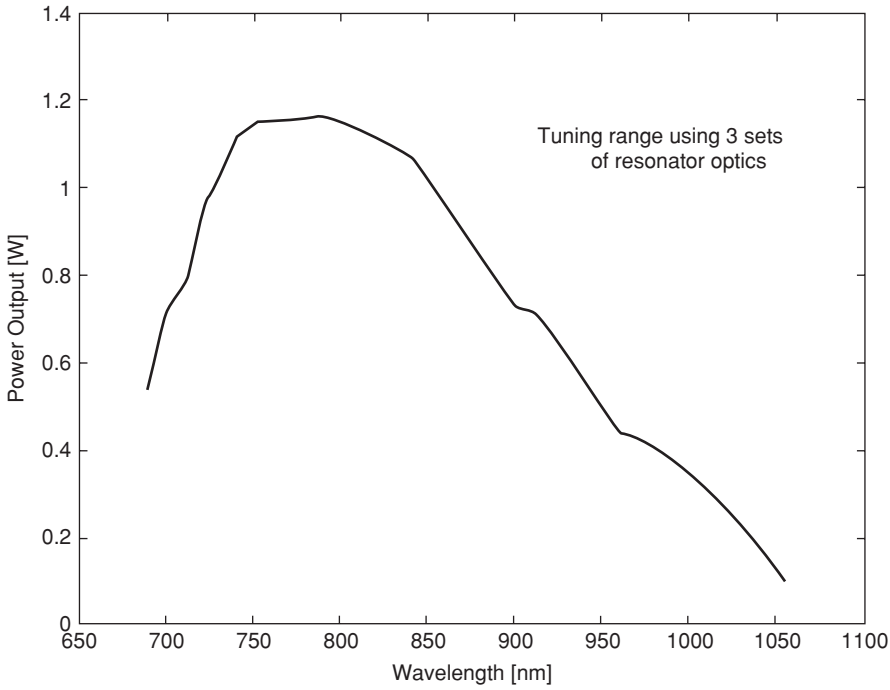


Fig. 2.27. Typical output power and spectral range of a Ti:sapphire laser pumped by a 5 W argon-ion laser (Schwartz Electro-Optics)

For pulsed solid-state lasers as pump source, output energies range from a few mJ at repetition rates of around 1 kHz, to 100 mJ per pulse at 20 pps.

Figure 2.28 displays the oputput of a Ti:sapphire laser pumped at 1 kHz by a frequency-doubled Nd:YLF laser which had an average output of 1.7 W at 527 nm. The pump pulses had a duration between 200 and 300 ns, whereas the Ti:sapphire laser yielded output pulses of 10–12 ns duration. This pulse shortening is characteristic of gain switched operation. The curves shown in Fig. 2.28 correspond to different sets of resonator mirrors.

With diode-pumped frequency-doubled Nd:YLF and Nd:YAG lasers as pump sources, very compact, all solid-state Ti:sapphire lasers can be designed [2.130–132]. The exceptionally broad gain band width of Ti:sapphire lasers can be exploited to generate extremely short pulses. The generation and amplification of mode-locked pulses is an important application of Ti:sapphire lasers and will be discussed in Chap. 9.

2.5.3 Cr:LiSAF

In the late 1980s, a family of fluorides was developed by Lawrence Livermore National Laboratory, which can serve as hosts for chromium. The crystals included Cr^{3+}:$LiSrAlF_6$ (LiSAF), which has a tuning range from 780 to 920 nm and an excited

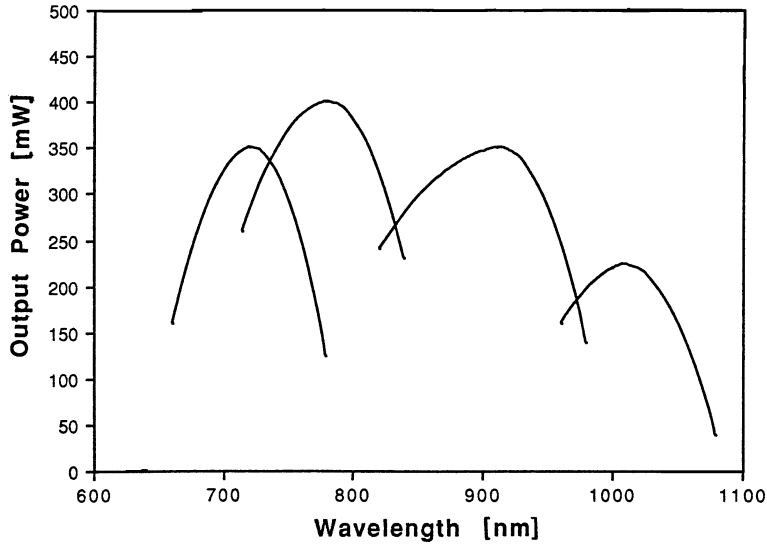


Fig. 2.28. Tuning range of a Ti:sapphire laser pumped by a Nd:YLF laser at 1 kHz [2.129]

lifetime of 67 μs [2.133] and Cr^{3+}:$LiCaAlF_6$ (LiCAF), which has a tuning range from 720 to 840 nm and a lifetime of 170 μs [2.134]. Since the peak emission of LiSAF is four times larger than LiCAF, it generally performs better, and most of the recent laser work has concentrated on LiSAF.

The LiSAF host crystal is uniaxial and the Cr^{3+} emission has been shown to be strongly π-polarized ($E \,||\, c$). The absorption and emission spectra are displayed in Fig. 2.29 [2.133]. The peak of the $^4T_2 \rightarrow {}^4A_2$ emission occurs at 830 nm and has a cross section of 4.8×10^{-20} cm^2. Very large laser rods with diameters up to 25 mm have been fabricated from crystals grown by the Czochralski technique.

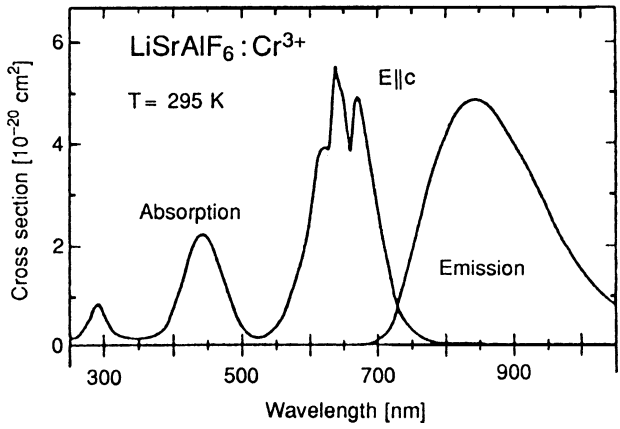


Fig. 2.29. Absorption and emission spectra of Cr:LiSAF [2.133]

Table 2.11. Comparison of relevant laser parameters for Cr:LiSAF and Ti:Sapphire

	Cr:LiSAF	Ti:Sapphire
Peak wavelength (nm)	850	790
Linewidth (nm)	180	230
Emission cross section (10^{-19} cm^2)	0.5	4.1
Fluorescence lifetime (μs)	67	3.2
Refractive index	1.41	1.76
Scattering loss (cm^{-1})	0.002	0

A comparison of important laser parameters of Cr:LiSAF with those of Ti:sapphire is shown in Table 2.11 [2.133, 134]. Peak emission of LiSAF is at a slightly longer wavelength as compared to Ti:sapphire, but there is a good overlap between the spectra. Actually, the output from mode-locked Ti:sapphire oscillators has been amplified by Cr:LiSAF amplifiers [2.135]. The gain bandwidth is narrower, but still comparable to Ti:sapphire. The major differences between the two crystals is the emission cross section, fluorescent lifetime, and the thermal and mechanical properties. While the gain of Cr:LiSAF is approximately one order of magnitude lower than that of Ti:sapphire, it has a long enough lifetime of 67 μs to permit efficient flashlamp pumping.

LiSAF is a rather soft and mechanically weak crystal with properties more related to glass than the far superior Ti:sapphire crystal. A comparison of the thermal and physical properties of LiSAF and glass is provided in Table 2.12 [2.136]. An important design consideration in using LiSAF crystals is the maintenance of the proper pH value of the cooling water for liquid-immersed laser rods. For example, at a pH value of 5, the material has a dissolution rate which is 100 times higher than that of YLF. However, at a pH value around 7, the dissolution rate is on the same order as YLF and phosphate glass.

Unlike Ti:sapphire, flashlamp pumping of Cr:LiSAF is fairly straight-forward due to the relatively long lifetime of the upper state level and the excellent overlap of the absorption bands with the emission of flashlamps. LiSAF can also be pumped with AlGaInP diodes at 670 nm [2.137, 138]. The product of emission cross section and upper state lifetime is sufficiently high ($\sigma\tau_f$) to facilitate a low cw laser threshold.

Table 2.12. Comparison of thermal and physical properties of LiSAF and glass

	Cr:LiSAF	Glass
Thermal shock resistance (W/m$^{1/2}$)	≈0.4	≈0.4
Fracture strength (kg/mm^2)	3.9	5
Thermal expansion coefficient ($\times 10^{-6}$/°C)	22	11.4
Young's modulus (Gpa)	100	50
Microhardness (kg/mm^2)	197	≈500
Fracture toughness (MPam$^{1/2}$)	0.4	0.45
Thermal conductivity (W/m K)	3.09	0.62

Laser action has even been achieved by pumping highly doped crystals at the wings of the absorption profile at 752 nm with AlGaAs diodes [2.139].

Cr:LiSAF has found applications as a flashlamp or diode-pumped laser source with tunable output around 850 nm. The broadband emissions of Cr:LiSAF makes this crystal attractive for the generation and amplification of femtosecond mode-locked pulses. Of particular interest is a diode-pumped, all solid-state tunable source for femtosecond pulse generation [2.140–142]. As will be discussed in Chap. 9, systems have been developed which range from small diode-pumped Cr:LiSAF mode-locked oscillators to very large flashlamp-pumped amplifier stages with rod diameters up to 25 mm.

2.5.4 Tm:YAG

Thulium and thulium-sensitized holmium lasers have outputs in the 2 μm region, a wavelength of interest for coherent radar systems, remote sensing, and medical applications. The possibility of pumping Tm-doped crystals with readily available powerful GaAlAs laser diodes at 785 nm has stimulated interest in these materials. Representative crystals of this class of three-level lasers are Tm:YAG [2.145–147], Tm:YAP [2.151], Tm:YLF [2.143, 144] Ho:Tm:YAG [2.30], and Ho:Tm:YLF [2.152–154]. In the singly doped crystals, laser radiation is produced by the Tm^{3+} ion at 2 μm. In the doubly doped crystals, pump radiation is absorbed by the thulium ion, and by a cross-relaxation process energy is transferred to the holmium ion. Laser emission occurs at 2.1 μm between the $^5I_7$ and $^5I_8$ levels in holmium.

As an example of these tunable lasers in the 2 μm region, we will consider diode-pumped Tm:YAG. It seems to be the preferred crystal for a number of applications. Although Ho:Tm:YAG has a larger cross section as compared to Tm:YAG, it generally has poorer output performance because of increased losses introduced by up conversion from the upper laser level [2.146, 148]. However, impressive performance levels at room temperature have been obtained in Ho:Tm:YLF with output energies up to 125 mJ at single frequency [2.152]. This crystal has lower up conversion losses as compared to Ho:Tm:YAG. Also the extremely long lifetime of the upper laser level of 14 ms provides high energy storage capability for Q-switch operation at low repetition rates.

In the previous section we saw that tunability of solid-state lasers was achieved by the 3d electron of the transition metal ions Cr^{3+} and Ti^{3+}. In Tm^{3+}:YAG, the considerable phonon broadening and high multiplicity of the Stark levels of the 4f electron provides relative broad tunability around 2 μm.

The relevant energy levels and transitions of Tm:YAG are shown in Fig. 2.30. Pump radiation at 785 nm transfers Tm^{3+} ions from the $^3H_6$ ground state into the $^3H_4$ level of Tm. From the $^3H_4$ pump level the ions relax down to the upper laser level $^3F_4$. Laser action takes place between level $^3F_4$ and the lower laser level, which lies within the $^3H_6$ ground-state manifold. Output radiation is around 2 μm.

At high Tm concentrations, cross-relaxation between adjacent ions can occur, whereby the excitation is undergoing the transition $^3H_4 \rightarrow {}^3F_4$, while an unexcited ion simultaneously undergoes the transition $^3H_6 \rightarrow {}^3F_4$. This process leaves two

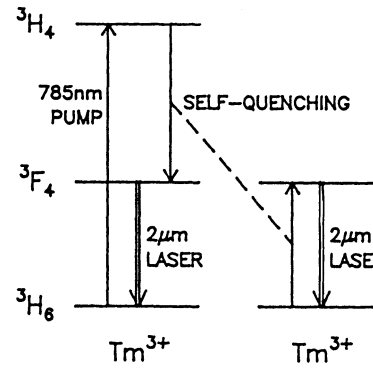


Fig. 2.30. Energy levels and pumping diagram for Tm:YAG [2.149]

Tm^{3+} ions in the upper laser level $^3F_4$ for every ion originally excited. In other words, two ions in the upper laser level are generated for every pump photon absorbed. At typical concentration levels of 3–12% Tm^{3+}, the quantum efficiency of pumping into the $^3F_4$ state is nearly two.

The fluorescence spectrum of Tm:YAG is shown in Fig. 2.31. The peak emission is at 2.02 μm and the bandwidth of fluorescence is about 400 nm. Tunability is typically from 1.87 to 2.16 μm. The absorption spectrum of Tm:YAG is centered at 785 nm and has a linewidth of 4 nm, which makes pumping attractive with GaAlAs diodes. Pertinent laser parameters are summarized in Table 2.13 [2.155]. Compared to Nd:YAG, the disadvantages of Tm:YAG are the higher threshold to overcome the residual population in the ground level and the two orders of magnitude smaller gain cross section. Since the lower laser level is in the ground-state manifold and therefore, partially populated, quasi-three-level lasers require stronger pump intensities or they require cooling to reduce the population in the lower laser level.

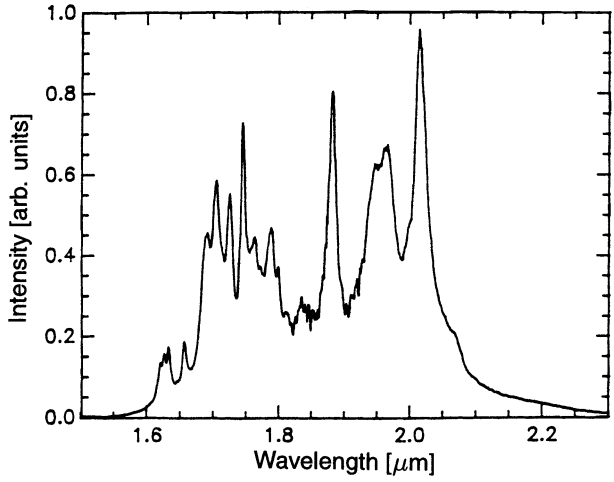


Fig. 2.31. Fluorescence spectrum for Tm:YAG [2.149]

Table 2.13. Material parameters of Tm:YAG [2.149, 155]

Pump wavelength	780–785 nm
Peak laser wavelength	2.02 μm
Effective cross section at 25°C	2×10^{-21} cm^2
Fluorescence lifetime	10 ms
Tunability	1.87−2.16μm

The rather dramatic improvement in laser performance when the Tm:YAG crystal is operated at reduced temperature is illustrated in Fig. 2.32. Also shown is the output dependence of Ho:Tm:YAG on temperature. Because of the more complete three-level nature of this material, the temperature dependence is even stronger than in Tm:YAG.

Instead of pumping Tm:YAG at the peak absorption line, sometimes "wing pumping" at 805 nm is employed. The lower absorption coefficient at that wavelength provides a longer pathlength in the crystal, which is advantageous in high power lasers for better heat removal and reduced thermal loading. Also, pump diode performance and reliability is improved because at the longer wavelength the aluminum concentration in GaAlAs is lower. In an end-pumped 3 mm diameter by 55 mm long Tm:YAG rod, a cw output of 115 W was achieved by pumping at 805 nm with 460 W of cw pump power [2.147]. The output was achieved by maintaining the crystal temperature at 3°C.

Side-pumping of a 3 mm diameter and 105 mm long, 3%-doped Tm:YAG rod produced 120 W cm power [2.145]. The active region of the Tm:YAG crystal was only 65 mm long. Diffusion-bonded, undoped end caps prevented absorption losses by the unpumped region of the laser rod. The 785 nm output from three diode arrays was coupled to the laser crystal through a compound parabolic concentrator. The maximum optical-to-optical conversion efficiency was 25%, and output vs input had a slope efficiency of 31%.

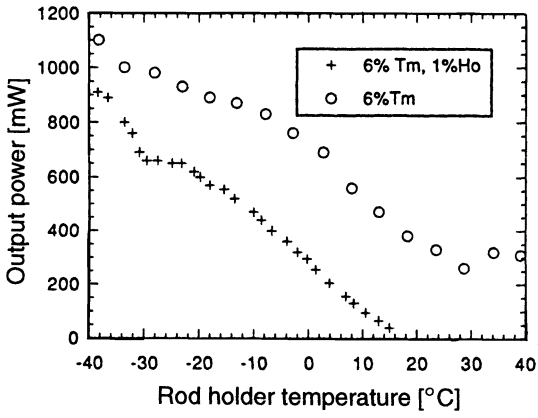


Fig. 2.32. Output power of Tm:YAG and Tm:Ho:YAG as a function of temperature [2.155]

Besides Tm:YAG, the crystal Tm:YLF has been frequently used to produce 2μm radiation [2.143, 144]. For example, a 3.5%-doped Tm:YLF slab, side-pumped by diode bars at 792 nm, generated 28 W of output at a pump power of 170 W. Threshold was 63 W and the slope efficiency was 25%.

2.6 Yb:YAG

Although Yb:YAG has been known for decades, interest was not very high in this material since it lacks any pump bands in the visible spectrum. The crystal has only a single absorption feature around 941 nm. With conventional pump sources such as flashlamps, the threshold is very high, which eliminated this material from any serious consideration. With the emergence of powerful InGaAs laser diodes that emit at 941 nm, the picture has changed completely and Yb:YAG has become an important laser material [2.156]. The relevant energy level diagram of Yb:YAG is very simple and consists of the $^2F_{7/2}$ lower level and $^2F_{5/2}$ excited state manifolds separated by about 10,000 cm^{-1}. The laser wavelength is at 1.03 μm, a representative emission spectrum for a 5.5 at.% doped sample is shown in Fig. 2.33.

The laser transition $^2F_{5/2}$–$^2F_{7/2}$ has a terminal level 612 cm^{-1} above the ground state (see Fig. 2.34). The thermal energy at room temperature is 200 cm^{-1}; therefore, the terminal state is thermally populated making Yb:YAG a quasi-three level system. By comparison, the terminal laser level in Nd:YAG is about 2110 cm^{-1} above the ground state. Being a quasi-three-level laser, Yb:YAG absorbs at 1.03 μm unless it is pumped to inversion. At room temperature the thermal population of the lower laser level is about 5.5%. The absorbed pump power per volume needed to achieve

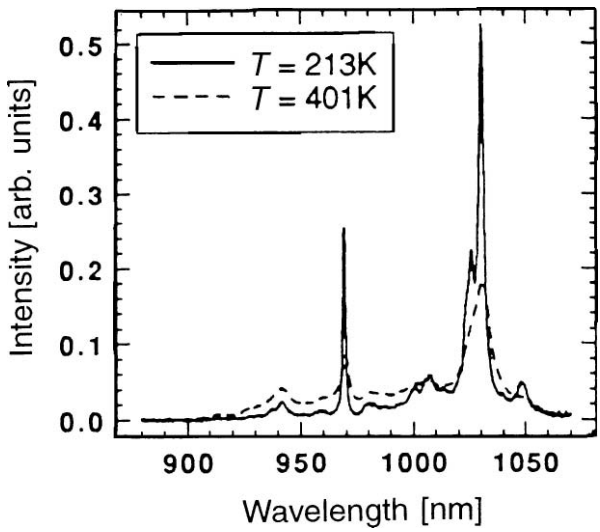


Fig. 2.33. Emission spectra of Yb:YAG with 5.5 at.% doping [2.157]

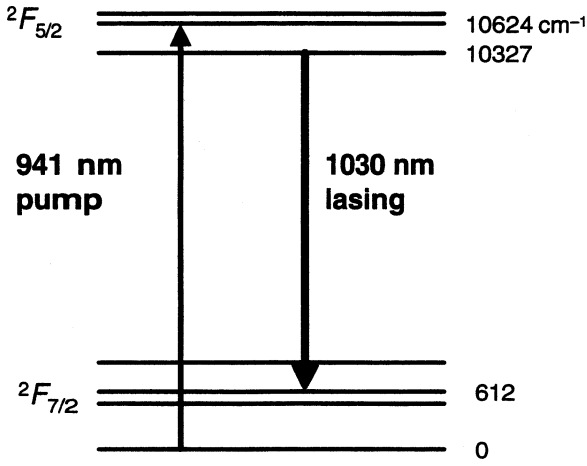


Fig. 2.34. Relevant energy levels in Yb:YAG

and maintain transparency at the laser wavelength is $I = f_a n_t h\nu_p/\tau_f$, where f_a is the fraction of the total ion density n_t occupying the lower laser level, $h\nu_p$ is the energy per pump photon, and τ_f is the lifetime of the upper level. With $f_a = 0.055$, $n_t = 1.38 \times 10^{20}$ cm^{-3} at 1% doping, $h\nu_p = 2.11 \times 10^{-19}$ J, and $\tau_f = 0.95$ ms, the absorbed pump power needed to reach inversion is 1.7 kW/cm^3. Of course, a higher power density is required to overcome optical losses and reach laser threshold, and for an efficient operation the laser has to be pumped about five to six times above threshold. Typically, in this laser, small volumes of material are pumped on the order of 10 kW/cm^3.

Yb:YAG performance is strongly dependent on temperature and can be improved by cooling the crystal, which reduces the thermal population and increases the stimulated emission cross section from 2.1×10^{-20} cm^2 at room temperature to twice this value at 220 K.

Figure 2.35 illustrates the dependence of optical efficiency, i.e., the conversion of pump light into laser output, on temperature [2.158]. In this laser a thin disk, about 0.4-mm thick, is pumped with fiber-coupled laser diodes in a multiple-path arrangement. The Yb:YAG crystal is mounted on a heat sink which could be cooled to low temperature. Two different pump sources were evaluated. With the smaller diode array the efficiency increased from 45% at room temperature to 64% at -74°C. With the larger pump source the efficiency changes from 38% at room temperature to 55% at -65°C. At this low temperature the output was 100 W for the 183 W pump. At the more typical operating temperature of -9°C for this laser, a pump power of 225 W was needed to generate the same output. Clearly, laser efficiency and cost of the pump source can be traded for overall system efficiency which includes power and cost for refrigeration. Quite noticeable is the high optical-to-optical efficiency which can be achieved in these lasers.

The strong temperature dependence of Yb:YAG requires an aggressive thermal management to avoid high temperatures.

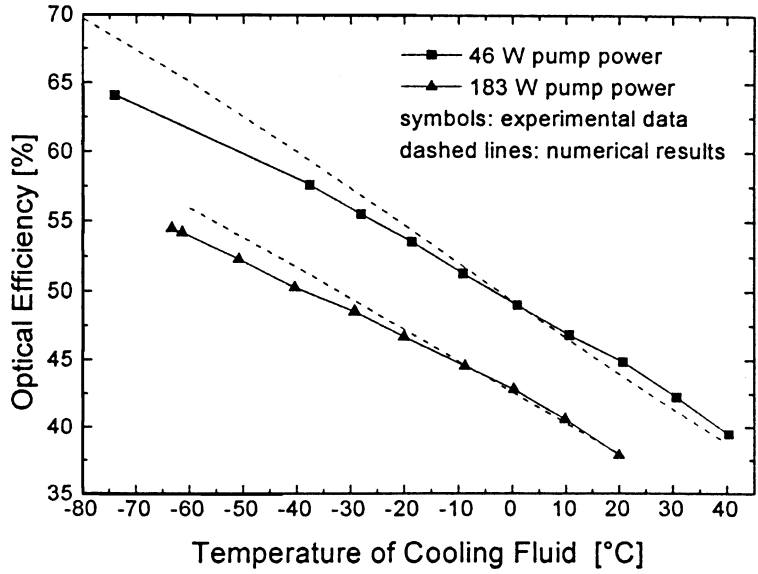


Fig. 2.35. Optical efficiency vs. temperature for Yb:YAG at two different pump powers [2.158]

In most of the large systems built to date the temperature of the crystal is maintained between -10°C and 20°C depending on the particular design and mode of operation. To maintain the laser crystal at such a temperature under intensive pump radiation requires, as a minimum, some kind of refrigeration.

Despite these obvious drawbacks, Yb:YAG has a number of redeeming features which motivated the development of very powerful systems. Pumping of Yb:YAG with an InGaAs pump source produces the smallest amount of crystal heating compared to any other major laser system. Actually the pump radiation in this material generates only about one-third of the heat compared to Nd:YAG. The fractional thermal loading, i.e., the ratio of heat generated to absorbed energy is around 11% for Yb:YAG pumped at 943 nm and 32% for Nd:YAG pumped at 808 nm. This substantially reduced thermal dissipation is the result of a very small energy difference between the photons of the pump and laser radiation. This quantum defect or Stokes shift is 9% in Yb:YAG versus 24% in Nd:YAG. The thermal load generated in a laser medium is of primary concern for high-power applications. The reduced thermal heat load can potentially lead to higher-average-power systems with better beam quality than possible with Nd:YAG. Other unique advantages of Yb:YAG are an absorption bandwidth of 18 nm for diode pumping, which is about 10 times broader than the 808 nm absorption in Nd:YAG. This significantly relaxes temperature control needed for the diode pump source. Yb:YAG has a long lifetime of 951 μs, which reduces the number of quasi-cw pump diodes required for a given energy per pulse output. As will be discussed in Chap. 6, since laser diodes are power limited, a long fluorescence time permits the application of a long pump pulse that, in turn, generates a high-energy output. Important materials parameters of Yb:YAG are listed in Table 2.14.

Table 2.14. Pertinent material parameters for Yb:YAG

Laser wavelength	1030 nm
Radiative lifetime at room temperature	951 μs
Peak emision cross section	2.1×10^{-20} cm^2
Peak absorption wavelength	941 nm
Pump bandwidth at 941 nm	18 nm
Doping density (1% at.)	1.38×10^{20} cm^3

Besides overcoming the initial absorption of Yb:YAG that is determined by the quasi-three-level structure, a high pump intensity is also required because of the rather small cross section of Yb:YAG which results in a large saturation intensity of 9.7 kW/cm^2 and a saturation fluence of 9.2 J/cm^2. For cw operation good extraction efficiency requires an intra-cavity intensity higher than the saturation density, and in pulsed operation the internal fluence has to exceed the saturation fluence.

The presence of only one excited-state manifold eliminates problems associated with excited-state absorption and up-conversion processes. Despite the quasi-three-level behavior of Yb:YAG, the obvious advantages of very low fractional heating, broad absorption at the InGaAs wavelength, long lifetime combined with high conductivity, and tensile strength of the host crystal have raised the prospect of high-power generation with good beam quality.

The major interest lies in large systems at the kilowatt level for industrial applications.

Different pump schemes, such as end- and side-pumping of a small rod, or face-pumping of a thin disk, have been tried with Yb:YAG lasers to meet the requirements of efficient thermal management and generation of high pump intensities. The various approaches all produced laser oscillators with output powers in excess of 1 KW.

In a side-pumped configuration, 1kW of cw power was obtained from an oscillator containing a 3 mm diameter and 30 mm long 1.5 at.% Yb:YAG crystal [2.159]. Threshold was at 1 kW, and with an optical-to-optical slope efficiency of 25% the maximum output was achieved at 5 kW pump input. The rod cooling temperature was held at 18°C. From the 0.21 cm^3 volume of the rod, follows a volumetric power density of 24 kW/cm^3 at the maximum input power. This power density is far in excess of the initial 1.7 kW/cm^3 pump investment required to bleach the crystal because of its quasi three-level nature. This explains why at very high output powers quasi-three-level lasers behave like four-leval systems.

Different resonator mirrors were tested and output mirrors with reflectivities between 50 and 68% produced about the same maximum output. From these values and a rod cross-sectional area of 0.21 cm^2 follows a power density inside the crystal between 43 and 75 kW/cm^2 (see Sect. 3.3). This is about a factor four to seven times the saturation density for Yb:YAG and thus assures good extraction efficiency.

In the end-pumped configuration, the output radiation from a stack of diode bars is collimated and funneled into the front end of a 2 mm diameter and 60 mm long rod [2.160]. The crystal is doped at a low concentration of 0.44% such that the absorption path is long and heat removal can take place along the barrel of the

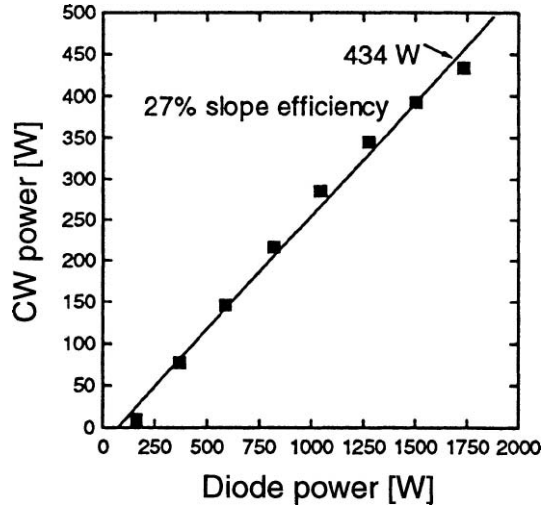


Fig. 2.36. cw output power as a function of diode power of an end-pumped Yb:YAG [2.160]

rod. The crystal temperature was maintained at 0°C with a water–alcohol mixtrue. Figure 2.36 illustrates the performance of the system, in which up to 434 W in cw mode was achieved.

In an extension of this work, two end-pumped 0.7%-doped Yb:YAG rods with undoped diffusion-bonded ends yielded 1080 W average power with 27.5% optical-to-optical efficiency[2.161].

Extremely small volumes, on the order of a few mm^3, are pumped in the thin-disk approach [2.158, 162, 163]. In this design, disks with a thickness of typically (0.3–0.4) mm are pumped from the front in a multiple pass active mirror design. The disks, mounted on a cold finger, are cooled from the backside. The pump beam is typically 2.5–7 mm in diameter. The discs are heavily doped up to 11%. At a temperature of 1°C an output power of 264 W was measured for one particular setup. Electrical input power to the diodes was 2060 W which gives an electrical to optical efficiency of 12.8%.

A thin 8% Yb:YAG disk with one side mounted on a heat sink generated cw output power of 1070 W with 48% optical efficiency[2.164].

In general, the efficiency of quasi-three level Yb:YAG lasers is comparable to the overall efficiency obtained in large Nd:YAG systems; however, the much reduced heat load in Yb:YAG permits generation of comparable outputs in much smaller laser crystals.

A number of crystals have been doped with Yb, in particular apatite crystals, but YAG is favored for power scaling because it has excellent thermomechanical properties.